RSC Advances

PAPER

View Article Online
View Journal | View Issue

Cite this: *RSC Adv.*, 2025, **15**, 3497

New 8-hydroxyquinoline-based azo dyes as highly sensitive colorimetric chemosensors for nickel cation†

Sefiu Olalekan Olaleye,[ab] Sunday Olakunle Idowu,*[a] Shakil Ahmed[c] and Maria Aqeel Khan*[b]

A new series of sensitive 8-hydroxyquinoline azo-compounds (**S1–S8**) as sensors was synthesized by diazotization and diazo-coupling, and these compounds were characterized through UV, FTIR, ^{1}H-NMR, ^{13}C-NMR and ESI-MS investigations. The UV-visible spectral data revealed that Ni^{2+} was sensed by compounds **S2**, **S3**, **S4**, and **S6**, producing colour changes ranging from violet to orange, and exhibited bathochromism of +8, +67, +63, and +85 nm, respectively. Optimized conditions included a mixture of ethanol/water (4 : 1) solvent system; pH 4 for compounds **S3**, **S4**, and **S6**, and pH 8 for compound **S2**; reaction time of 2 min; and a stoichiometric ratio of 3 : 1. The limits of detection for the Ni^{2+} cation demonstrated by the dyes were in the range of 0.012–0.038 μM using UV-visible spectroscopy, which is lower than the permissible value of Ni^{2+} (1.2 μM) in drinking water specified by the United States Environmental Protection Agency. Intra-day and inter-day accuracies of the Ni^{2+} cation spiked in tap and underground water (in terms of relative errors) were less than 5%, while precisions were less than 4.0% (RSD). The accuracy and precision of chemosensor-based analyses were comparable to those of the inductively coupled plasma mass spectrometry (ICP-MS) method. Colour changes of paper strips with sensors **S2**, **S3**, **S4**, and **S6** ranged from orange to violet in the presence of nickel. Infrared analysis confirmed that sensors interacted with Ni^{2+} through nitrogen and hydroxyl moieties of quinoline. Thus, an easy-to-use, highly sensitive, and low-cost method for analyzing nickel in water samples was established.

Received 2nd December 2024
Accepted 15th January 2025

DOI: 10.1039/d4ra08510h

rsc.li/rsc-advances

1. Introduction

Nickel is an essential element with daily requirements within the range of 25 to 35 μg,[1] and living cells are harmed upon its homeostatic imbalance. It is required in the active sites of many crucial enzymes, including catalytic processes, carbon monoxide dehydrogenases, hydrogenases, acetyl-coenzymes, superoxide dismutases, and acireductone dioxygenases.[2,3]

Nickel enters into water bodies through manufacturing and metallurgical activities, mining, incineration and combustion of fossil fuels; catalyst and chemical production; and effluents from industry (EFSA, 2015). Excessive exposure to Ni can raise the plasma level above the normal range of 12–85 μg L^{-1},[4] which can lead to acute pneumonitis, dermatitis, asthma, cancer of the lung and sinus, adverse effects on blood and kidneys, and other disorders of the respiratory and central nervous systems.[5] Hence, there is a need to rapidly monitor the nickel levels in environmental samples.

Instrumental methods, such as inductively coupled plasma-mass spectrometry (ICP-MS), inductively coupled plasma-optical emission spectrometry (ICP-OES), inductively coupled plasma-atomic emission spectrometry (ICP-AES), atomic absorption spectrometry (AAS), atomic absorption spectrometry (AES), flame atomic absorption (FAA), flame atomic emission (FAE), and graphite furnace atomic absorption, that are used to determine nickel ion concentration suffer from several drawbacks. Although the ICP methods offer the advantages of multiple element analysis, a large analytical range, and low detection limits, they are not suitable for low-resource economies because of their high equipment cost, high operating cost (argon), complex operation, and high level of staff expertise.[6] On the other hand, AAS, AES, FAE, and FAA are relatively cost-effective, but they are single-element procedures that are poorly selective and sensitive.[6] Therefore, there is a need for the development of chemosensors that offer simple instantaneous detection, low cost, high sensitivity, and selectivity in the analysis of Ni.[7]

[a]*Department of Pharmaceutical Chemistry, Faculty of Pharmacy, University of Ibadan, Orita UI, Ibadan, 200284, Nigeria. E-mail: olakunleid@yahoo.com*

[b]*Third World Center for Science and Technology, H. E. J. Research Institute of Chemistry, International Center for Chemical and Biological Sciences, University of Karachi, Karachi, 75270, Pakistan. E-mail: drmaria.aqeel@iccs.edu*

[c]*Industrial Analytical Center, International Center for Chemical and Biological Sciences, University of Karachi, Karachi, 75270, Pakistan*

† Electronic supplementary information (ESI) available. See DOI: https://doi.org/10.1039/d4ra08510h

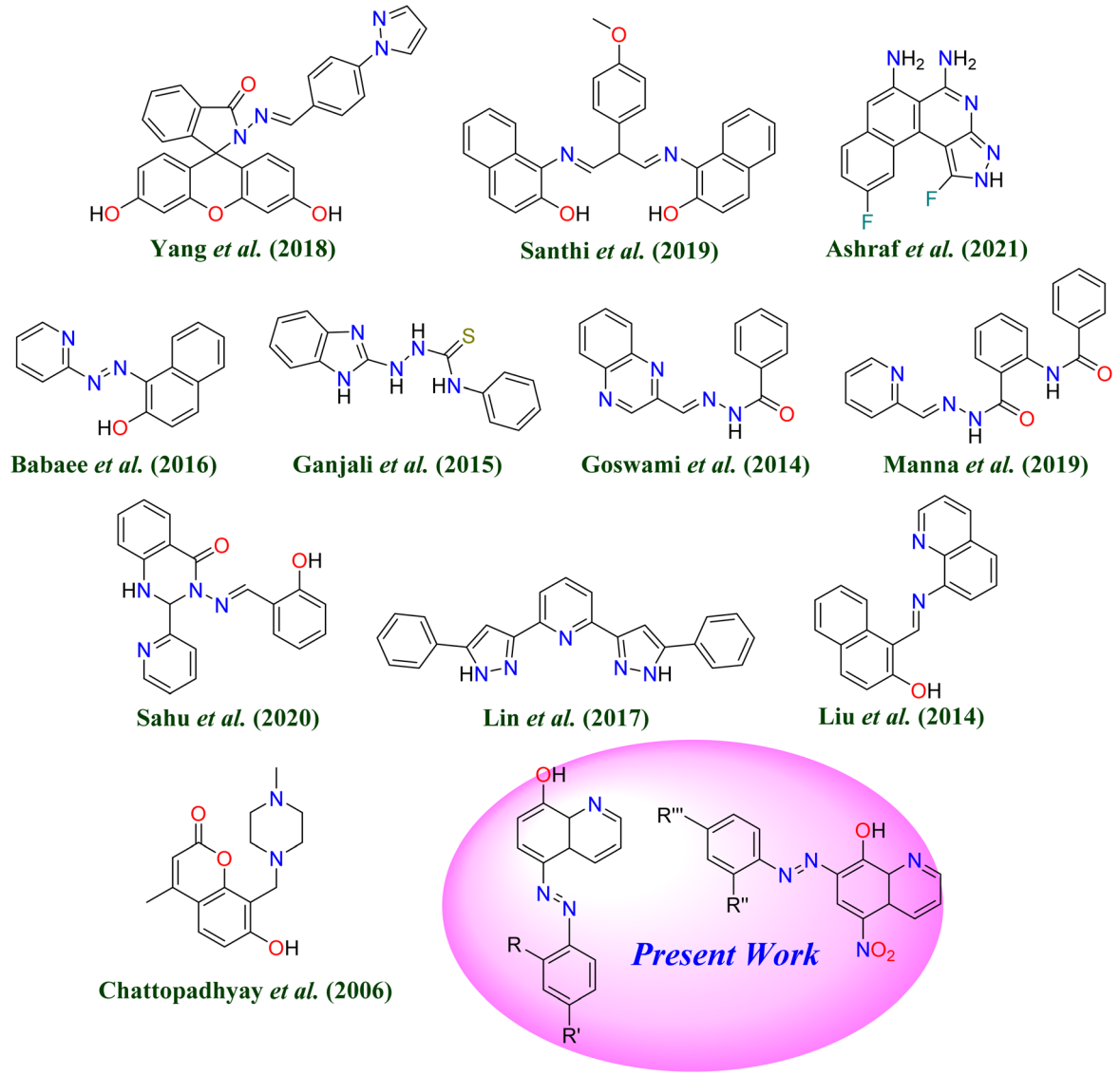

Fig. 1 Chemical structures of some prior chemosensors for nickel.

Azo compounds have found applications in different endeavours, especially in chemosensor designs. Sancenon and co-workers (2003)[8] reported that the introduction of an azo bridge in chemosensors enhances their chromogenic characteristics, which enhances their suitability as sensors. Azo derivatives of 8-hydroxyquinoline have been reported as chemosensors for Pb^{2+},[9] Cd^{2+},[10] Hg^{2+},[10] CN^{-},[11] and F^{-} ions.[12] Prior evidences revealed that there are very few studies in the literature on sensors for nickel ion detection, as depicted in Fig. 1,[13–15] and the use of azo-based derivatives of 8-hydroxyquinoline has not been widely explored for sensing nickel ions. In addition, some of the reported prior chemosensor-based methods utilized milieus, such as dimethyl sulfoxide (DMSO),[16,17] *N*,*N*-dimethylformamide (DMF),[18] acetonitrile (ACN),[19,20] and tetrahydrofuran (THF).[21] These solvents are not only eco-unfriendly, but are also relatively expensive and not readily available for chemosensing experiments. Hence, this study reports a new class of 8-hydroxyquinoline-based azo dyes as highly sensitive colorimetric chemosensors for the simple, inexpensive, and rapid analysis of nickel in ethanol/water mixtures.

2. Experimental

2.1 General information, material and methods

Sulfanilamide, 2-methoxy-4-nitroaniline, 4-methoxy-2-nitroaniline, aniline, 2-amino-4-nitrophenol, 2,3-dimethylaniline, 8-amino-2-naphthol, sodium nitrite, 8-hydroxyquinoline, hexane, ethyl acetate, dichloromethane, acetone, acetonitrile, ethanol, methanol, DMF, DMSO, glacial acetic acid, concentrated hydrochloric acid, concentrated trioxonitrate(v) acid, concentrated sulphuric acid, potassium hydroxide, potassium acetate, copper sulphate, lead nitrate, zinc sulphate, calcium sulphate, mercuric acetate, lithium chloride, magnesium sulphate, sodium sulphate, potassium sulphate, silver nitrate, cobalt(II) chloride, ferric chloride, ferrous sulphate, aluminium chloride, nickel(II) acetate, and pH buffers were used in this

study. All the reagents were obtained from BDH, Poole, England. Thin-layer chromatography (TLC) was developed on pre-coated silica gel aluminum plates (Kieselgel 60F254, E. Merck, Germany). A hotplate magnetic stirrer purchased from Thermo Fisher Scientific, US, was used. ^{1}H-NMR and ^{13}C-NMR spectra were recorded on Bruker Avance spectrometers (UK) at 500, 600, and 800 MHz. UV-Vis spectral data were obtained on a Nicolet Evolution 300 UV-visible spectrophotometer (Thermo Electron Corporation, US). FTIR spectral data were obtained on a Nicolet iS20 FTIR spectrometer (Thermo Fisher Scientific, US). ESI-MS measurements were recorded on an AmaZon speed ESI-ion trap mass spectrometer (Bruker, UK). The ICP-MS 7700 Series (Agilent Technologies, US) was used. The pH of the solution was obtained on a pH meter (Hanna, US). The melting point was obtained on an M-560 (BUCHI, Switzerland) instrument.

2.2 Synthesis

2.2.1 Preparation of nitroxoline. The method of Voronin *et al.* (1976)[22] was used with modifications. 2 g (13.8 mmol) of 8-hydroxyquinoline was added to a stirring mixture of 19 mL of water and 1 mL of concentrated sulphuric acid at a temperature of 25 °C. 1.7 g (24.6 mmol) of sodium nitrite dissolved in 5 mL of water was added dropwise for 30 min. The reaction was allowed to stay for 3 h. Afterwards, the solution was neutralized to a pH of 8 with 11 M sodium hydroxide. Then, it was acidified again with glacial acetic acid to pH 4.0. The precipitate formed was filtered and washed with distilled water. While in a paste form, 9 mL of concentrated nitric acid was added to the precipitates in 20 mL of water at 30 °C. The reaction was maintained at this temperature for 3 h. The mixture was cooled to 10 °C, and the pH was readjusted to 8 with 11 M sodium hydroxide. It was then acidified to pH 4 by the addition of glacial acetic acid (AcOH). The precipitates were filtered and washed until no yellow color was observed. Then, it was air-dried and recrystallized in an acetone/water system. The spectral data of nitroxoline was matched with that given in the literature.

2.2.2 Synthesis of compounds S1 and S2. Compounds **S1** and **S2** were synthesized by a one-pot two-step reaction (diazotization and diazo coupling). 1.05 mmol of activated sodium nitrite dissolved in 5 mL of water was added into solutions of 1.05 mmol of sulfanilamide or 2-methoxy-*p*-nitro aniline in water : concentrated hydrochloric acid (10 : 1). The reaction was allowed to stay for 30 min in an ice bath. Afterwards, 1.05 mmol of nitroxoline dissolved in 20 mL of glacial acetic acid was introduced into the diazonium solutions, while maintaining the reaction at a temperature of less than 5 °C for 3 h. The reaction progress was monitored with TLC, and the reaction pH was adjusted to 6–7 with 6 M potassium acetate solution after a reaction time of 2 h. The ensuing colored solid was filtered, washed with water, and dried at room temperature. Pure compound **S1** was obtained by dissolution of the crude product in ethyl acetate and recrystallization by adding *n*-hexane until turbidity was observed. Compound **S2** was purified by column chromatography through gradient elution with hexane and EtOAc.

2.2.3 Characterization of compounds S1 and S2

*4′-[2-(8-Hydroxy-5-nitroquinolin-7-yl)diazen-1-yl]benzene-1-sulfonamide (**S1**).*

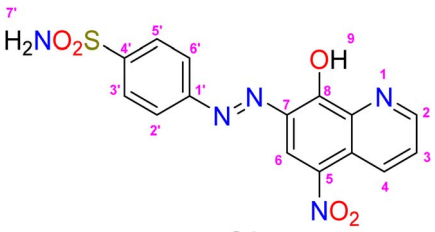

S1

Orange solid; yield: 74%; FTIR (ATR, ν, cm^{-1}): 3400, 3300, 3200, 2981, 1609 (C=N), 1574, 1506 (N=N), 1396 (C–O); ^{1}H-NMR (500 MHz, DMSO-d_6, δ, ppm): 9.37 (d, $J_{2,3}$ = 8.7 Hz, 1H, H-2), 9.04 (d, $J_{4,3}$ = 4.4 Hz, 1H, H-4), 8.89 (s, 1H, H-6), 8.12 (d, $J_{2',3'/6',5'}$ = 8.2 Hz, 2H, H-2′/H-6′), 8.06–8.02 (m, 3H, *overlapped*, H-3, H-3′/H-5′), 7.54 (s, 2H, sulfonamide NH_2, *exchanges with* D_2O); ^{13}C-NMR (600 MHz, DMSO-d_6, δ, ppm): 162.5 (C), 153.3 (C), 147.1 (CH), 145.5 (C), 138.9 (C), 135.9 (C), 134.4 (CH), 132.1 (CH), 127.1 (CH), 126.5 (C), 124.8 (C), 123.0 (CH), 117.8 (CH); MS (ESI, *m*/*z*): 374 [M$^+$+H].

*7-[(2-(2′-Methoxy-4′-nitrophenyl)diazen-1-yl]-5-nitroquinolin-8-ol) (**S2**).*

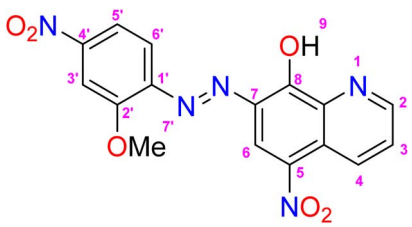

S2

Red solid; yield: 71%; FTIR (ATR, ν, cm^{-1}): 3300, 3081, 2850, 1610 (C=N), 1569, 1506 (N=N), 1384 (C–O); ^{1}H NMR (500 MHz, DMSO-d_6, δ, ppm): 9.23 (d, $J_{2,3}$ = 8.5 Hz, 1H, H-2), 8.87 (s, 1H, H-6), 8.68 (dd, $J_{4,3}$ = 4.8 Hz, $J_{4,2}$ = 1.3 Hz, 1H, H-4), 7.94 (d, $J_{6',5'}$ = 2.4 Hz, 1H, H-6′), 7.91 (dd, $J_{5',6'}$ = 8.7 Hz, $J_{5',3'}$ = 2.4 Hz, 1H, H-5′), 7.72–7.58 (m, 2H, *overlapped*, H-3, H-6′), 4.07 (s, 3H, OCH_3-7′); ^{13}C-NMR (800 MHz, DMSO-d_6, δ, ppm): 174.6 (C), 155.3 (C), 147.4 (CH), 146.9 (C), 146.7 (C), 138.1 (C), 132.7 (CH), 126.5 (CH), 125.1 (CH), 125.0 (C), 119.2 (CH), 117.2 (CH), 116.4 (CH), 107.9 (C), 55.9 (CH_3); MS (ESI, *m*/*z*): 370 [M$^+$+H].

2.2.4 Synthesis of compounds S3 to S8. 1.40 mmol of sodium nitrite dissolved in 5 mL water was gradually added into a stirring solution of aromatic amines (1.40 mmol in 20 mL HCl). The reaction was maintained at a temperature below 5 °C. After 30 min, 1.40 mmol of 8-hydroxyquinoline dissolved in 1 M KOH : water (1 : 1), was introduced dropwise into the diazonium solutions. The reaction was allowed to stay for 3 h at the temperature. The progress of the reaction was continuously monitored with TLC. The pH was adjusted to 6–7 with 1 M KOH solution. The colored solid formed was filtered, washed with water, and dried at room temperature. Dyes **S3–S5**, **S7** and **S8** were purified in an acetone/water mixture, while pure

compound **S6** was obtained from an ethyl acetate/*n*-hexane system.

2.2.5 Characterization of compounds S3 to S8

*5-[2-(2′-Methoxy-4′-nitrophenyl)diazen-1-yl]quinolin-8-ol (**S3**).*

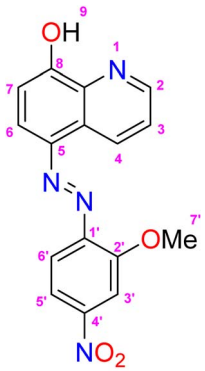

S3

Red solid; yield: 80%; FTIR (ATR, ν, cm^{-1}): 3300, 3112, 2820, 1614 (C═N), 1506 (N═N), 1360 (C–O); ^{1}H-NMR (500 MHz, DMSO-d_6, δ, ppm): 9.33 (d, $J_{2,3}$ = 8.4 Hz, 1H, H-2), 9.01 (d, $J_{5',6'}$ = 4.1 Hz, 1H, H-5′), 8.03 (s, 1H, H-3′), 7.99 (d, $J_{6,7}$ = 2.8 Hz, 1H, H-6), 7.94 (d, $J_{4,3}$ = 2.0 Hz, 1H, H-4), 7.89 (d, $J_{6',5'}$ = 8.8 Hz, 1H, H-6′), 7.80 (dd, $J_{3,2}$ = 8.5 Hz, $J_{3,4}$ = 4.1 Hz, 1H, H-3), 7.28 (d, $J_{7,6}$ = 10.2 Hz, 1H, H-7), 4.10 (s, 3H, OCH_3-7′); ^{13}C-NMR (800 MHz, DMSO-d_6, δ, ppm): 158.7 (C), 156.1 (C), 149.1 (C), 149.0 (CH), 145.8 (C), 145.1 (C), 139.4 (CH), 137.5 (C), 136.4 (CH), 136.1 (C), 107.5 (CH), 56.7 (CH_3); MS (ESI, *m*/*z*): 325 [M^++H].

*5-[2-(4′-Methoxy-2′-nitrophenyl)diazen-1-yl]quinolin-8-ol (**S4**).*

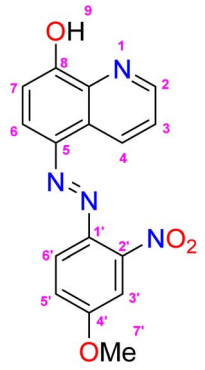

S4

Red solid; yield: 75%; FTIR (ATR, ν, cm^{-1}): 3244, 2821, 1611 (C═N), 1507 (N═N), 1361 (C–O); ^{1}H-NMR (500 MHz, DMSO-d_6, δ, ppm): 9.20 (d, $J_{2,3}$ = 8.5 Hz, 1H, H-2), 8.99 (d, $J_{4,3}$ = 4.0 Hz, 1H, H-4), 8.05 (d, $J_{6',5'}$ = 9.0 Hz, 1H, H-6′), 7.86 (d, $J_{6,7}$ = 8.5 Hz, 1H, H-6), 7.77 (dd, $J_{3,2}$ = 8.6, $J_{3,4}$ = 4.1 Hz, 1H, H-3), 7.66 (d, $J_{3',5'}$ = 2.7 Hz, 1H, H-3′), 7.37 (dd, $J_{5',6'}$ = 9.0 Hz, $J_{5',3'}$ = 2.8 Hz, 1H, H-5′), 7.24 (d, $J_{7,6}$ = 8.6 Hz, 1H, H-7), 3.93 (s, 3H, OCH_3-7′); ^{13}C-NMR (600 MHz, DMSO-d_6, δ, ppm): 161.0 (C), 158.4 (C), 149.2 (CH), 148.8 (C), 138.7 (C), 137.9 (C), 137.5 (C), 131.7 (CH), 127.5 (CH), 123.5 (C), 120.6 (CH), 118.9 (CH), 115.8 (CH), 112.0 (CH), 108.3 (CH), 56.6 (CH_3); MS (ESI, *m*/*z*): 325 [M^++H].

*5-[2-(7′-Hydroxynaphthalen-1-yl)diazen-1-yl]quinolin-8-ol (**S5**).*

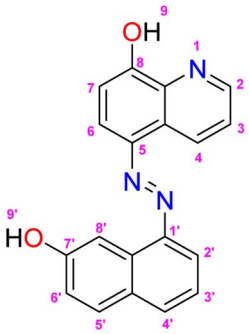

S5

Brown solid; yield: 78%; FTIR (ATR, ν, cm^{-1}): 3400, 2980, 1623 (C═N), 1504 (N═N), 1380 (C–O); ^{1}H-NMR (600 MHz, C_3D_6O, δ, ppm): 9.47 (dd, $J_{2,3}$ = 8.5 Hz, $J_{2,4}$ = 1.6 Hz, 1H, H-2), 8.98 (dd, $J_{4,3}$ = 4.1 Hz, $J_{4,2}$ = 1.6 Hz, 1H, H-4), 8.36 (d, $J_{8',6'}$ = 2.4 Hz, 1H, H-8′), 8.20 (d, $J_{6,7}$ = 8.4 Hz, 1H, H-6), 7.99 (d, $J_{4',3'}$ = 4.2 Hz, 1H, H-4′), 7.98 (d, $J_{2',3'}$ = 3.8 Hz, 1H, H-2′), 7.93 (d, $J_{5',6'}$ = 8.9 Hz, 1H, H-5′), 7.79 (dd, $J_{3,2}$ = 8.5 Hz, $J_{3,4}$ = 4.1 Hz, 1H, H-3), 7.44 (t, $J_{3',(2',4')}$ = 7.8 Hz, 1H, H-3′), 7.34 (d, $J_{7,6}$ = 8.4 Hz, 1H, H-7), 7.27 (dd, $J_{6',5'}$ = 8.8, $J_{6',8'}$ = 2.5 Hz, 1H, H-6′); ^{13}C NMR (600 MHz, C_3D_6O, δ, ppm): 157.3 (C), 157.2 (C), 149.9 (CH), 147.7 (C), 141.2 (C), 138.8 (C), 134.3 (CH), 133.3 (CH), 131.9 (CH), 130.8 (C), 130.6 (C), 128.3 (C), 124.1 (CH), 123.4 (CH), 119.9 (CH), 116.0 (CH), 113.2 (CH), 111.3 (CH), 105.3 (CH); MS (ESI, *m*/*z*): 316 [M^++H].

*5-[2-(2′-Hydroxy-5′-nitrophenyl)diazen-1-yl]quinolin-8-ol (**S6**).*

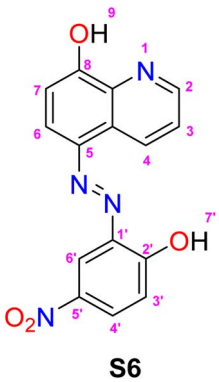

S6

Reddish-yellow solid; yield: 83%; FTIR (ATR, ν, cm^{-1}): 3300, 2971, 1622 (C═N), 1502 (N═N), 1348 (C–O); ^{1}H-NMR (500 MHz, C_3D_6O, δ, ppm): 9.24 (d, $J_{2,3}$ = 7.9 Hz, 1H, H-2), 9.01 (s, 1H, H-4, *partly split*), 8.78 (d, $J_{6',4'}$ = 2.6 Hz, 1H, H-6′), 8.35 (d, $J_{6,7}$ = 7.9 Hz, 1H, H-6), 8.32 (d, $J_{4',3'}$ = 6.9 Hz, 1H, H-4′), 7.88–7.83 (m, 1H, H-3), 7.34 (d, $J_{7,6}$ = 7.9 Hz, 1H, H-7), 7.31 (d, $J_{3',4'}$ = 8.7 Hz, 1H, H-3′); ^{13}C-NMR (800 MHz, C_3D_6O, δ, ppm): 156.7 (C), 150.2 (CH), 150.1 (C), 138.7 (C), 138.4 (C), 132.8 (C–H), 128.1 (C), 124.9

(CH), 119.5 (CH), 118.9 (CH), 111.6 (CH); MS (ESI, *m*/*z*): 311 [M^++H].

*5-[2-(2′,3′-Dimethylphenyl)diazen-1-yl]quinolin-8-ol (**S7**).*

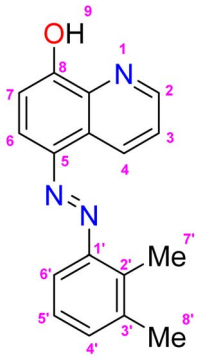

S7

Red solid; yield: 73%; FTIR (ATR, ν, cm^{-1}): 3600, 2950, 1577 (C=N), 1510 (N=N), 1379 (C–O); ^{1}H-NMR (500 MHz, DMSO-d_6, δ, ppm): 9.26 (dd, $J_{2,3}$ = 8.6 Hz, $J_{2,4}$ = 1.7 Hz, 1H, H-2), 8.93 (dd, $J_{4,3}$ = 4.2 Hz, $J_{4,2}$ = 1.7 Hz, 1H, H-4), 7.95 (d, $J_{6,7}$ = 8.5 Hz, 1H, H-6), 7.71 (dd, $J_{3,2}$ = 8.6 Hz, $J_{3,4}$ = 4.1 Hz, 1H, H-3), 7.59 (d, $J_{6',5'}$ = 8.0 Hz, 1H, H-6′), 7.29 (d, $J_{4',5'}$ = 7.3 Hz, 1H, H-4′), 7.22 (t, $J_{5',(4',6')}$ = 7.8 Hz, 1H, H-5′), 7.21 (d, $J_{7,6}$ = 7.8 Hz, 1H, H-7), 2.61 (s, 3H, CH_3-7′), 2.33 (s, 3H, CH_3-8′); ^{13}C-NMR (600 MHz, DMSO-d_6, δ, ppm): 158.1 (C), 150.7 (C), 148.8 (CH), 138.8 (C), 138.2 (C), 138.2 (C), 136.0 (C), 131.8 (CH), 131.6 (CH), 127.6 (C), 125.9 (CH), 123.1 (CH), 115.1 (CH), 113.1 (CH), 111.9 (CH), 19.6 (CH_3), 13.0 (CH_3); MS (ESI, *m*/*z*): 278 [M^++H].

*5-(Phenyldiazenyl)quinolin-8-ol (**S8**).*

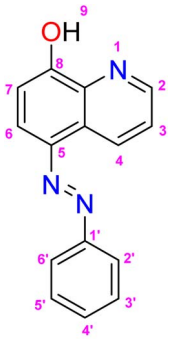

S8

Yellow solid; yield: 76%; FTIR (ATR, ν, cm^{-1}): 3433, 2930, 1621 (C=N), 1496 (N=N), 1404 (C–O); ^{1}H NMR (500 MHz, DMSO-d_6): δ 9.51 (d, $J_{2,3}$ = 8.5 Hz, 1H, H-2), 9.06 (dd, $J_{4,3}$ = 4.4 Hz, $J_{4,2}$ = 1.6 Hz, 1H, H-4), 8.06 (d, $J_{6,7}$ = 8.5 Hz, 1H, H-6), 8.01 (d, $J_{2',3'/6',5'}$ = 7.0 Hz, 2H, H-2′/H-6′), 7.90 (dd, $J_{3,2}$ = 8.6 Hz, $J_{3,4}$ = 4.4 Hz, 1H, H-3), 7.61 (t, $J_{3',2'/5',6'}$ = 8.2 Hz, $J_{3',4'/5',4'}$ = 6.7 Hz, 2H, H-3′/H-5′), 7.55 (t, $J_{4',(3',5')}$ = 7.5 Hz, 1H, H-4′), 7.40 (d, $J_{7,6}$ = 8.6 Hz, 1H, H-7); MS (ESI, *m*/*z*): 250 [M^++H].

2.3 Stock solution preparations for solvatochromic assessment and chemosensing studies

2.3.1 Dye stock solution. 5 mg of each dye (**S1–S8**) was weighed and dissolved in 10 mL of DMF in a volumetric flask to give solutions of 1.34–2.00 mM for solvatochromic assessment studies. For chemosensing studies, 5 mL of dye stock for solvatochromic assessment was diluted to 10 mL with DMF to produce 0.67–1.00 mM.

2.3.2 Metal salt solution. 2.0 mg of each of the metal salts was dissolved in 10 mL of deionized water to produce a final concentration of 200 ppm (200 mg L^{-1}).

2.4 Solvatochromic behaviours of compounds S1–S8

An aliquot of 100 μL of each dye stock solution was pipetted into eight different vials. The volume was made up to 5 mL with dichloromethane, methanol, ethanol, ethyl acetate, dichloromethane, acetonitrile, dimethylformamide, and dimethyl sulfoxide. The resultant concentrations of solutions of compounds **S1**, **S2**, **S3**, **S4**, **S5**, **S6**, **S7**, and **S8** were 26.8, 27.2, 30.8, 30.8, 31.8, 32.2, 36.2, and 40 μM, respectively. Baseline corrections of the UV-visible spectrometer were carried out with the aforementioned solvents (*i.e.*, methanol, ethanol, ethyl acetate, dichloromethane, acetonitrile, DMF, and DMSO). Then, the UV-visible scans of the solutions were recorded at 200 to 700 nm on the Thermo Electron Corporation Nicolet Evolution 300 UV-visible spectrophotometer with Vision Pro software.

2.5 Chemosensing screening

A volume of 500 μL of each metal ion solution (Cu^{2+}, Pb^{2+}, Zn^{2+}, Ca^{2+}, Hg^{2+}, Li^+, Mg^{2+}, Na^+, K^+, Ag^+, Co^{2+}, Fe^{3+}, Fe^{2+}, Al^{3+}, Ni^{2+}) (concentration of all salts is 200 ppm) was added into fifteen vials, followed by 100 μL of phosphate buffer and 100 μL of each dye. The mixtures were swirled gently for 10 seconds, and the vials were allowed to stay for 2 minutes before they were made up to 5 mL with ethanol and water (80 : 20, v/v). Baseline corrections of the UV-visible spectrometer were done with a mixture of ethanol, water, and phosphate buffer. The absorption spectra of the mixtures were measured from 200 to 700 nm, and overlaid for each dye. An ideal chemosensor was selected, along with metal ions that gave different colouration from others. The working analytical wavelength was determined by inspection of the overlaid spectra for wavelength, where there was a maximum difference in absorptivity in terms of hyperchromism and bathochromism.

2.5.1 Optimization studies of the sensor–nickel(II) reaction

Diluting the solvent for the sensor–nickel(II) reaction. An aliquot of 500 μL Ni^{2+}, 100 μL buffers (pH 8 for compound **S2** and pH 4 for compounds **S3**, **S4**, and **S6**), and 100 μL dye solution were added to vials and swirled for 10 seconds. This was then diluted to 5 mL with ethanol. The UV spectrum of the resulting solution between 200 and 700 nm was acquired. The procedure was repeated with methanol, acetone, DMSO, and deionized water as dilution solvents.

A mixture of 500 μL Ni^{2+}, 100 μL buffer, and 100 μL dye was made up to 5 mL with ethanol and water in the ratio of 20 to 80. The ethanol : water proportion was replaced with 40%, 50%, 60%, and 80% ethanol. The absorption scan was read at 200–700 nm after the baseline correction of the spectrophotometer.

Chelating time of the sensor–nickel(II) reaction. A volume of 500 μL of Ni^{2+} solution was added to an empty vial. This was

followed by introduction of 100 μL of buffer, and then 100 μL of the dye stock solution. After gently stirring the mixture, the effect of different times allowed for chelation to occur between nickel and dyes at 30 °C, was tested at 0, 2, 5, 10, 15, 20, 25, and 30 minutes. Then, ethanol and water (80 : 20) were added to the mixture to make a final volume of 5 mL. The absorbance was read at wavelengths of maximum absorption (λ_{max}); 448, 513, 470, and 497 nm for compounds **S2**, **S3**, **S4**, and **S6**, respectively. This was repeated with replicate samples.

2.5.2 Optimization studies of pH of the sensor–nickel(II) reaction medium. An aliquot of 100 μL of phosphate buffer at pH 4, 6, 7, 8, and 10 was separately added to five vials containing a mixture of 500 μL of Ni^{2+} solution and 100 μL dye solution before diluting to 5 mL with ethanol : water (80 : 20). The absorbance was read at λ_{max}: 448, 513, 470, and 497 nm for compounds **S2**, **S3**, **S4**, and **S6**, respectively. A duplicate determination was made in each case.

2.5.3 Determination of the stoichiometry for the formation of the complex. Using Job's plot of continuous variation,[23] into nine vials containing 0, 20, 25, 35, 50, 65, 75, 80, and 100 μL of compound **S2**, aliquots of an equimolar Ni^{2+} solution were added to make the volume up to 100 μL. Thereafter, 100 μL of buffer at pH 8 was added to each mixture and swirled for 10 seconds before making up the volume of each reaction mixture to 5 mL with ethanol and water (80 : 20). The absorbance was read at a maximum wavelength of 448 nm. The determination was done in replicates. The entire procedure was repeated with working concentrations of compounds **S6**, **S3**, and **S4**, and their absorbance measurements were taken at analytical wavelengths of 497, 513, and 470 nm, respectively.

2.5.4 Competition experiment for selectivity. A 20 μL volume of Ni^{2+} stock solution, equivalent to 3.21 μM, was spiked into vials containing 3.21 μM each of Ag^{+}, Pb^{2+}, Hg^{2+}, Li^{+}, Ca^{2+}, Mg^{2+}, K^{+}, Zn^{2+}, Al^{3+}, Na^{+}, Fe^{2+}, Fe^{3+}, Cu^{2+}, Co^{2+}, and a mixture of fourteen metal ions. A 75 μL quantity of compound **S2** was added, followed by 100 μL of buffer at pH 8. The mixture was swirled for 10 seconds and made up to 5 mL with ethanol : water (80 : 20). Determination was done in replicates, and the absorbance was read at 448 nm. Blank determinations with Ni^{2+} without other metal ions were carried out. The entire procedure was repeated with compounds **S6**, **S3**, and **S4**, and their absorbance measurements were taken at analytical wavelengths of 497, 513, and 470 nm, respectively.

2.5.5 Validation studies

Linearity of the response and construction of the calibration curve. Into vials, each containing 100 μL of phosphate buffer at pH 8, volumes of 0, 10, 20, 25, 30, 35, 40, and 50 μL from the Ni^{2+} stock solution were added, respectively. Then, 150 μL of compound **S2** solution was added to each vial. The mixtures were swirled for 10 seconds and allowed to stay for 2 minutes, then the ethanol : water (80 : 20, v/v) solvent system was added to make a 5 mL mixture. Absorbance readings were recorded at 448 nm, and three replicate determinations were done. A calibration line equation was generated from the average absorbance values, and a regression coefficient was obtained from the curve. The procedure was repeated for compounds **S3** (513 nm), **S4** (470 nm), and **S6** (497 nm).

Limit of detection (LOD), limit of quantitation (LOQ) and binding constant. A 150 μL volume of each dye solution (**S2**, **S3**, **S4**, and **S6**) was measured into vials containing 100 μL of phosphate buffer. The mixture was made up to 5 mL with ethanol : water (80 : 20, v/v). The procedure was done six times for each dye, and absorbance readings were recorded at 448, 513, 470, and 497 nm for compounds **S2**, **S3**, **S4**, and **S6**, respectively. The LOD was determined as $\frac{3\sigma}{s}$ and LOQ as $\frac{10\sigma}{s}$, where σ was the standard deviation from six blank determinations and s was the slope.

The binding constant was estimated from Benesi–Hildebrand's plot. $\frac{1}{A - A_o}$ was plotted against $\frac{1}{[Ni^{2+}]}$. A was the absorbance reading at different concentrations of Ni^{2+} solution, and A_o was the absorbance of the azo dye alone.

$$\text{Binding constant } (K) = \frac{\text{intercept}}{\text{slope}}$$

2.5.6 Water analysis

Preparation of water sample for analysis. Water samples were collected from two sources: tap water from the Third World Center for Science and Technology, the International Center for Chemical and Biological Sciences (ICCBS), University of Karachi, Pakistan; and underground water from Ayub Goth (Suparco Road), Gulshan-e-Hijri, Karachi East, Pakistan. Samples were transferred into thoroughly cleaned bottles and filtered twice to remove particulate matter.

Recovery studies. Accuracy and precision were the analytical parameters determined through recovery studies. Into quadruplicate samples of tap and underground water at two concentration levels of 1.607 and 3.215 μM of spiked Ni^{2+} solution, 100 μL buffer pH 4 and 150 μL of compound **S3** solution were added. The reaction mixture was swirled and set aside for 2 minutes. Thereafter, it was made up to 5 mL with an ethanol : water solution (80 : 20, v/v). This was repeated four times for each volume and water sample on three different days. The absorbance readings were recorded at 513 nm with a mixture of phosphate buffer, ethanol, and water as blank solvent. A three day recovery study was carried out, and the accuracy and precision were determined from the regression equation. Recovery studies using compounds **S2** and **S4** were carried out by spiking water samples with 3.215 and 5.626 μM of Ni^{2+} solution.

ICP-MS analysis. The level of Ni^{2+} present in the blank tap and underground water was assessed. A calibration curve was constructed using a standard nickel solution. Nickel ion concentrations of 1.607, 3.2147, and 5.626 μM were added into empty vials. The vials were made up to 5 mL of tap and underground water. The concentration of Ni^{2+} was determined by extrapolating on the calibration line of the standard Ni^{2+} solution prepared. This was performed in duplicate.

Test of equivalence of chemosensor probes and ICP-MS. The accuracy and precision of the two methods were compared with the Student's t-test and F-test, respectively, at $p < 0.05$, using the same water samples from tap and underground sources.

2.5.7 Synthesis of the nickel complex for FTIR studies. A weighed amount of 3.82 mg (0.0154 mmol) of nickel acetate dissolved in 5 mL of deionized water was added dropwise to 5.0 mg (0.0154 mmol) of compound **S3** dissolved in 5 mL of DMF over a period of 10 minutes. The reaction was made to proceed with constant stirring for 2 hours. The complex was obtained by filtration, which was then washed with deionized water and dried at room temperature. Complexes with compounds **S2**, **S4**, and **S6** were similarly synthesized in a 1 : 1 ratio.

2.5.8 Detection of nickel with a test strip coated with sensor S3 (paper strip test). Filter paper was cut into a 1 cm by 5 cm size. The paper was coated with sensor **S3** by immersion in compound **S3** solution. The paper was allowed to dry in air. The developed paper was dipped in a mixture of 200 μL of 0.2 g per L (0.8037 mmol L^{-1}) Ni^{2+} and 100 μL of phosphate buffer (pH 4).

3. Results and discussion

3.1 Synthesis of compounds S1–S8

From the illustration in Scheme 1, it can be observed that two different sets of chemosensors are prepared: set-I comprises compounds **S1** and **S2**, while set-II consists of compounds **S3–S8**. Products are obtained by utilizing a typical diazotization reaction, where corresponding diazonium salts are initially prepared *in situ via* treating substituted anilines or amino-naphthol (**I**) with sodium nitrite in acidic solution. Upon the addition of the coupling components (nitroxoline and 8-hydroquinoline), this preparation gave the corresponding diazo product. The formation of a colored product was indicated by colour changes of the diazonium solution from yellow upon adding the solution of coupling components. For set-II, the electrophilic substitution of diazonium ions (derived from substituted anilines) on the quinoline moiety occurred *para* to the hydroxyl group in compounds **S3–S8**. However, in compounds **S1** and **S2** (set-I), substitution took place at the carbon *ortho* to the phenolic group, with the *para* position being occupied by the nitro substituent (of nitroxoline). Nitroxoline (**II**) in turn was obtained by nitration reaction (electrophilic aromatic substitution) on 8-hydroquinoline (**III**).

3.2 Solvatochromism

3.2.1 UV-Vis spectra of azo compounds. The UV-visible spectral information of the azo compounds **S1–S8** in the various neat solvents, including ethyl acetate (EtOAc), methanol (MeOH), ethanol (EtOH), dichloromethane (CH_2Cl_2), dimethyl

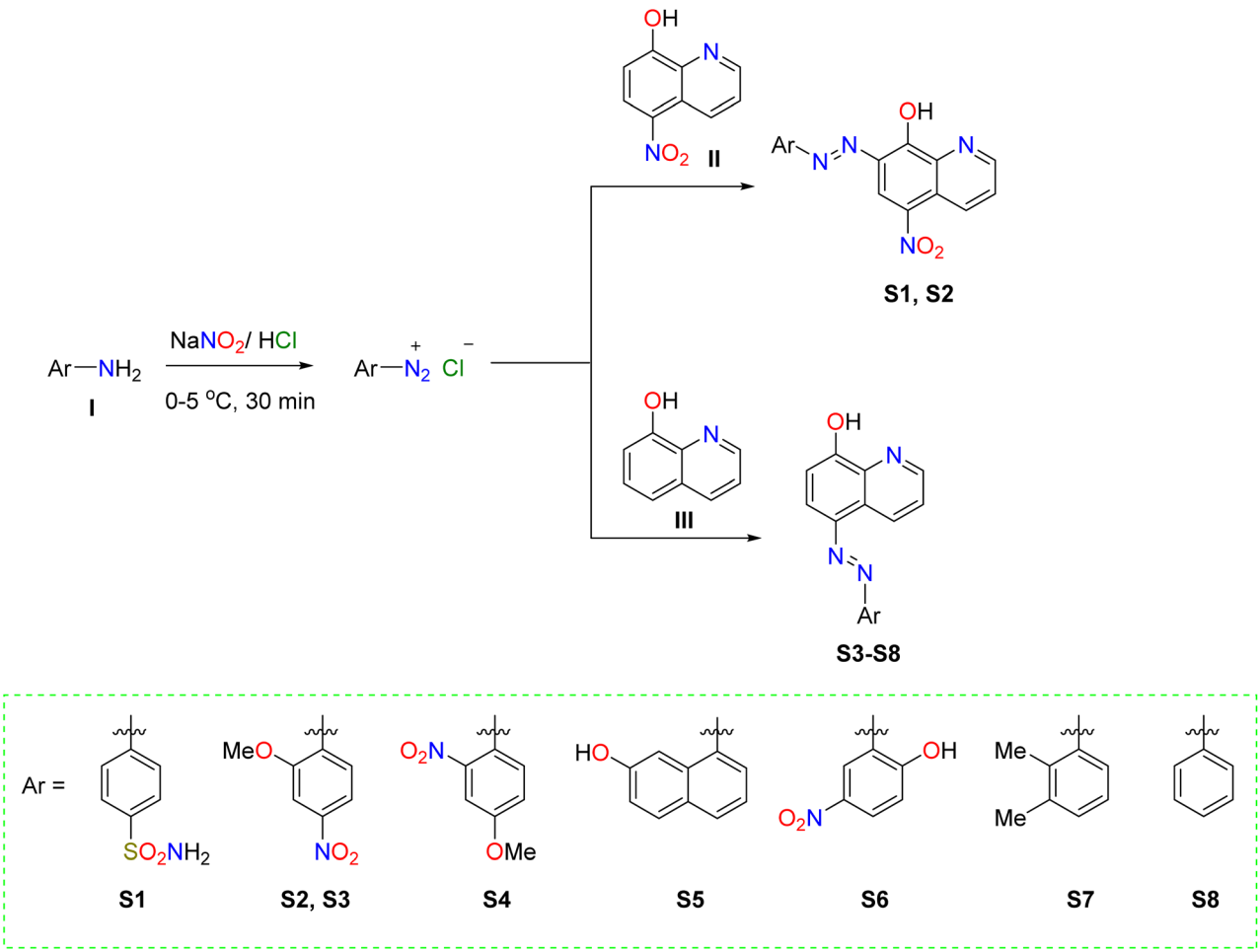

Scheme 1 Synthetic routes of compounds S1–S8.

Table 1 Absorption spectral data of compounds S1–S8 in solvents of various polarities s–shoulder.

	λ_{max} (nm), $\varepsilon_{max} \times 10^5$ M^{-1} cm^{-1} (log of ε_{max})						
Compound	MeOH	EtOAc	EtOH	DMSO	DMF	CH_2Cl_2	CH_3CN
S1	420, 0.11(4.05)	420, 0.10(3.99)	426, 0.14(4.13)	435, 0.12(4.07) 517, 0.09(3.97)s	437, 0.13(4.11) 525, 0.09(3.94)s	420, 0.08(3.92)	431, 0.17(4.24)
S2	430, 0.09(3.97) 502, 0.09(3.93)	438, 0.13(4.11) 495, 0.08(3.92)	426, 0.13(4.13)	445, 0.12(4.07) 555, 0.12(4.09)s	442, 0.14(4.16) 554, 0.13(4.11)s	437, 0.15(4.17)	436, 0.17(4.22)
S3	430, 0.09(3.95)	419, 0.16(4.20)	439, 0.10(4.01)	654, 0.29(4.46)	651, 0.34(4.54)	421, 0.15(4.18) 576, 0.07(3.82)s	628, 0.29(4.46)
S4	400, 0.14(4.15)	403, 0.23(4.37)	409, 0.18(4.25)	419, 0.20(4.30) 517, 0.13(4.10)s	413, 0.16(4.22) 530, 0.19(4.27)s	400, 0.19(4.27)	400, 0.16(4.19) 514, 0.08(3.90)s
S5	420, 0.07(3.84)	419, 0.13(4.10)	424, 0.10(3.99)	448, 0.13(4.12)	430, 0.12(4.07)	421, 0.13(4.10)	416, 0.11(4.04)
S6	442, 0.10(3.97)	413, 0.08(3.91)	413, 0.10(4.01)	413, 0.11(4.05)	425, 0.09(3.93) 525, 0.16(4.19)s	413, 0.10(3.99)	409, 0.12(4.09) 512, 0.08(3.88)s
S7	380, 0.14(4.15)	380, 0.17(4.23)	383, 0.13(4.12)	394, 0.14(4.14)	390, 0.11(4.05) 479, 0.08(3.89)s	379, 0.16(4.19)	376, 0.12(4.09)
S8	382, 0.07(3.86)	380, 0.07(3.85)	385, 0.07(3.84)	394, 0.08(3.91)	393, 0.08(3.89) 497, 0.04(3.56)s	380, 0.08(3.90)	376, 0.08(3.88)

s – shoulder.

sulfoxide (DMSO), acetonitrile (ACN), and *N*,*N*-dimethylformamide (DMF), is shown in Table 1. A cursory look at the data indicates two major absorption peaks at long and short wavelengths. The long wavelengths ranging from 400 to 656 nm are low energy bands arising from π–π* electronic transitions due to dye–solvent interactions. The bands at high energy between 229 and 315 nm are the shorter wavelengths. In general, the high absorptivity of the dyes at shorter wavelengths can be due to chromophoric moieties bound to the 8-hydroxyquinoline nucleus in addition to the azo functional group (–N=N–).

3.2.2 Azo-hydrazone tautomerism. Tautomerism is a phenomenon exhibited by azo-naphthols, whereby there is an intramolecular rearrangement of the acidic hydrogen of phenol to the azo group. The spectral fashion of the compounds is common with azo-hydrazone tautomeric rearrangement.[24] The hydrazone form of the azo dye is attributed to the low-energy band, and the azo form is peculiar to the high-energy band. Scheme 2 illustrates the azo-hydrazone transformation.

Further indication of tautomerism was evident from the ^{13}C-NMR data of compounds **S2** and **S5**, recorded in deuterated dimethyl sulfoxide (Fig. S6 and S15, given in ESI†). Compound **S2** showed a peak at δ 174.6, while compound **S5** exhibited a peak at δ 174.0 for C-8 in both compounds. However, all the other azo compounds produced peaks in the range of δ 157.2 to 162.0 when characterized in the same deuterated solvent. Thomas and Adegoke (2022)[24] demonstrated that the carbon atom holding the hydroxyl group has a chemical shift of around δ 160.0 in azo form, while the shift occurs at δ 170.0 for ketonic carbon in the hydrazone form. The ketonic carbon peak was completely absent when compound **S5** was analyzed in deuterated acetone (Fig. S14, ESI†). This indicates that the compound exists mainly in the azo form in acetone.

Typically, the hydrazone tautomer is associated with the low-field signal in the ^{1}H-NMR spectrum.[25] The peak at δ 17.3, with an integral of 0.95 in the ^{1}H-NMR spectrum of compound **S5** in deuterated DMSO (Fig. S15†), was attributed to the β-hydrogen of N–H of the hydrazone tautomer of compound **S5**. This lends credence to the fact that compound **S5** exists predominantly as a hydrazone tautomer. On the other hand, the downfield peak was conspicuously absent in the ^{1}H-NMR spectrum of compound **S2**; this might be due to the rapid equilibrium shift to the azo form.

3.2.3 Effect of solvent and substituent on absorption. Representative absorption spectra of the dyes are shown in Fig. 2. The presence of different substituents on the 8-hydroxyquinoline-based azo compounds facilitates interaction with the solvents. These solute–solvent interactions resulted in different solvent colourations (Table 2).

Absorption of compound **S8** was negligible in all the solvents in the visible region due to the absence of a substituent. However, there was a shoulder at 484 nm in DMF. Moving from ethyl acetate to hydrogen bond acceptor (HBA) solvents such as DMSO and DMF, there was a positive solvatochromism of 13 nm, but a blue shift (−4 nm) was observed in acetonitrile. This might be a result of weak interaction with the acetonitrile. The addition of weak activators, methyl groups, at position-2 and -3 in compound **S7** did not reveal a noticeable difference in the spectral pattern when compared

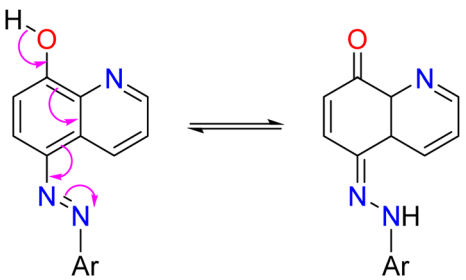

Scheme 2 Tautomeric transformation of azo to hydrazone form.

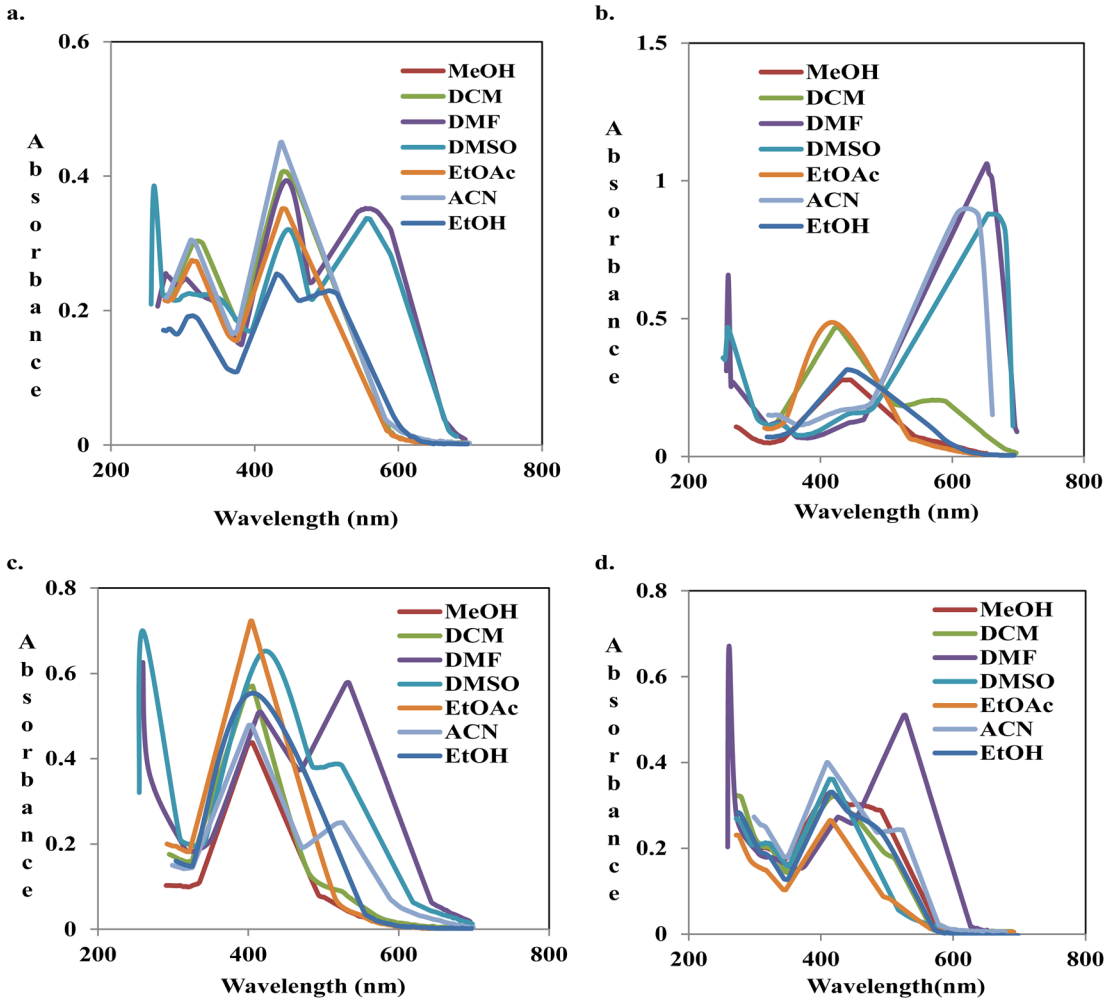

Fig. 2 Overlaid spectra of compounds S2 (a), S3 (b), S4 (c) and S6 (d) in different solvents.

Table 2 Colours of compounds in various solvents

	Colours in solvents						
Compound	EtOAc	MeOH	EtOH	CH_2Cl_2	DMSO	ACN	DMF
S1	Yellow	Yellow	Yellow	Yellow	Orange	Yellow	Orange
S2	Orange	Pink	Orange	Orange	Purple	Yellow	Purple
S3	Yellow	Yellow	Orange	Green	Blue	Blue	Blue
S4	Yellow	Yellow	Yellow	Yellow	Orange	Pink	Deep pink
S5	Yellow	Yellow	Yellow	Yellow	Orange	Pink	Pink
S6	Yellow	Orange	Yellow	Yellow	Yellow	Orange	Pink
S7	Yellow	Yellow	Yellow	Orange	Orange	Pink	Pink
S8	Yellow	Yellow	Yellow	Yellow	Yellow	Yellow	Yellow

to compound **S8**. Meanwhile, the shoulder band in the visible region of DMF was more pronounced. The observed shoulder in the spectra of compounds **S7** and **S8** might be a result of enol formation.

The dielectric constant of solvents is in the following order: EtOH > CH_2Cl_2 > EtOAc. There was no difference in the absorption maxima of compound **S6**, but the absorptivity decreased steadily. Moving to a more polar solvent, MeOH, there was bathochromism ($\Delta\lambda$ = +29 nm) and hyperchromicity. A non-hydrogen bond donor solvent, *e.g.*, DMF, enhances the hydrazone formation, although compound **S6** exists primarily in the azo form in the solvent. The absorption spectrum indicated $\Delta\lambda$ = +83 nm, relative to what was acquirable in EtOH. The *ortho*-hydroxyl group of the benzenoid could be involved in intramolecular interaction with the α-nitrogen of the azo-linkage due to its proximity to the group (Fig. 3A).

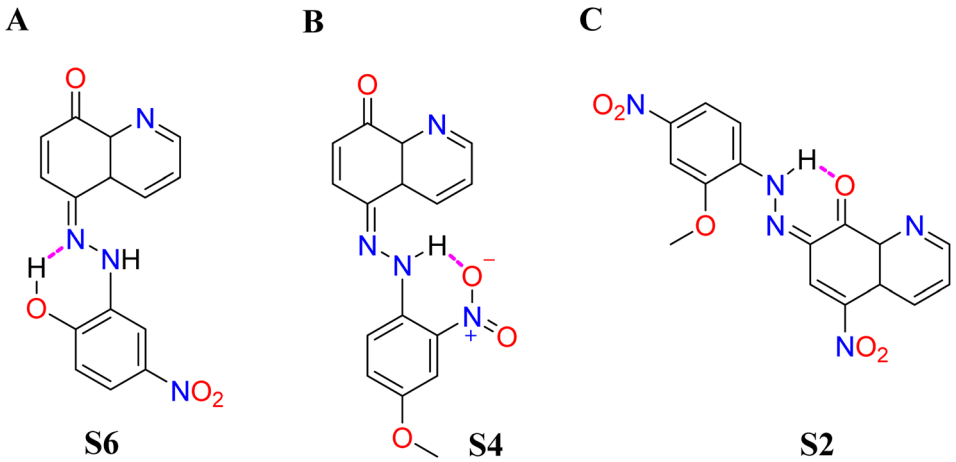

Fig. 3 Intramolecular hydrogen bond formation in hydrazones of compounds (A) **S6**, (B) **S4**, and (C) **S2**.

Hence, it is not likely to be free for hydrogen bond formation with non-hydroxylic solvents. The long-wavelength absorption observed in DMF was probably due to interaction *via* the β-proton in the hydrazone (Fig. 4A).

In moving from methanol to DMSO and DMF, compound **S5** indicated a red shift of +28 and +10 nm, respectively. DMSO, a solvent with a greater dielectric constant than DMF, interacted strongly *via* inter-charge transfer (ICT) in terms of hydrogen bonding with β-hydroxyl in the naphthalene moiety.

Compounds **S3** and **S4** are structural isomers; the two azo dyes differ in the position of $-NO_2$ and $-OCH_3$ group on the benzenoid nucleus. In EtOAc, compound **S3** revealed an absorption band at 419 nm. Moving to CH_2Cl_2, a slight positive solvatochromism of +2 nm, with a shoulder peak at 576 nm, was observed. There was bathochromism of $\Delta\lambda = +9$ nm in methanol, a more polar solvent. A noticeable red shift of +209, +232, and +235 nm with marked hyperchromicity was indicated in ACN, DMF, and DMSO, respectively. With the spectral pattern, equilibrium was shifted towards hydrazone formation in these solvents. The hydrogen bonding with DMF and other non-hydroxylic solvents through hydrazone β-proton likely accounted for the observation (Fig. 4B). The pull effect of *para*-nitro to azo and the push phenomenon of the hydroxyl group of the quinoline might also be a contributing factor to the chromophoric elongation. There was only a slight difference in the absorption maxima on increasing polarity from EtOAc to MeOH.

On the contrary, in hydrogen bond acceptor (HBA) solvents, compound **S4** indicated an absorption maximum at 530 nm in DMF and shoulder peaks at 514 and 507 nm in DMSO and ACN, respectively. Compound **S4** has a NO_2 group *ortho* to the N=N linkage and OCH_3 at the *para*-position. The proximity of NO_2 and azo-linkage results in intramolecular hydrogen bonding to give a six-membered ring, thus stabilizing the hydrazone form, as shown in Fig. 3B. A similar trend was observed by Rashidnejad and co-workers when they compared the solvatochromism of arylazo-5HQ with 8HQ derivatives.[26] Interaction with hydrogen bond donor solvents (MeOH, EtOH, and CH_2Cl_2) might result in dipole–dipole interaction, unlike in compound **S3**.

There was a slight difference in the spectral behaviours of compound **S1** in CH_2Cl_2, EtOAc, MeOH, and EtOH. There was a bathochromic shift moving to DMF (+15 nm), ACN (+11 nm),

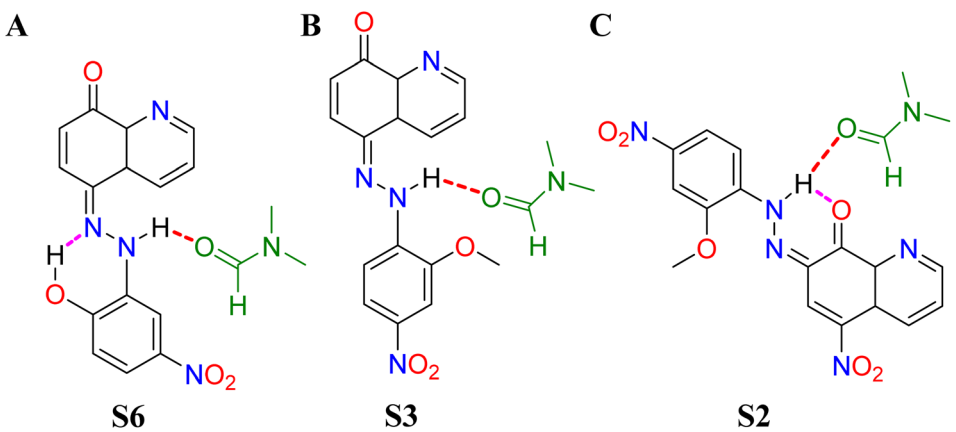

Fig. 4 Intermolecular hydrogen bond formation (in red line) between DMF (in green color) and the hydrazone moiety of compounds (A) **S6**, (B) **S3**, and (C) **S2**.

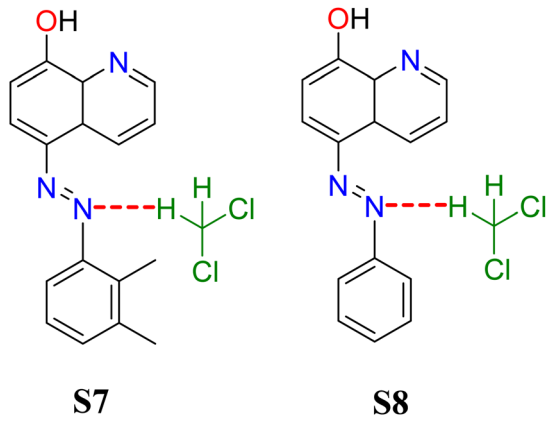

Fig. 5 Hydrogen bond formation (in red line) between CH_2Cl_2 (in green color) and compounds (A) **S7** and (B) **S8**.

and DMSO (+17 nm). As the polarity increased in the order of EtOAc > CH_2Cl_2 > MeOH > DMF > DMSO, there was a proportional shift of maximum absorption of compound **S2** to longer wavelengths. Phenolic hydroxyl, in compound **S2**, was not available for bonding with HBA due to intramolecular hydrogen bonding (Fig. 3C). In each of the solvents, the wavelength of the maximum absorption in compound **S2** was more than that in compound **S1**. This might be connected to the pull–pull effect of the two NO_2 moieties on the structure of compound **S2**.

It is noteworthy that the presence of a strong electron-withdrawing substituent like NO_2 stabilizes the hydrazone tautomer by reducing the electron density of the aromatic ring structure. Compounds **S2**, **S3**, **S4**, and **S6** indicated prominent tautomerism in DMSO and DMF (Fig. 2). All the 8-hydroxyquinoline azo dyes except compounds **S7** and **S8** revealed a significant decline in the absorption intensity of almost nine-fold in CH_2Cl_2 in the visible region. This could have been due to the strong solvent–solute interaction of dyes (**S7** and **S8**) with CH_2Cl_2 *via* hydrogen bonding formation with –N=N– (Fig. 5).

3.3 Chemosensor screening

The addition of nickel to the pink solution of compound **S2** and the yellow solutions of compounds **S3**, **S4**, and **S6** gave colour changes to yellowish orange, deep violet, and orange, respectively. The overlaid absorption spectra of the resulting nickel–dye solutions of compounds **S3** (Fig. 6), **S2**, **S4,** and **S6** (Fig. S28, S29 and S31 ESI†) gave red shifts of +8, +67, +63 and +85 nm, respectively, relative to other cations: Cu^{2+}, Pb^{2+}, Zn^{2+}, Ca^{2+},

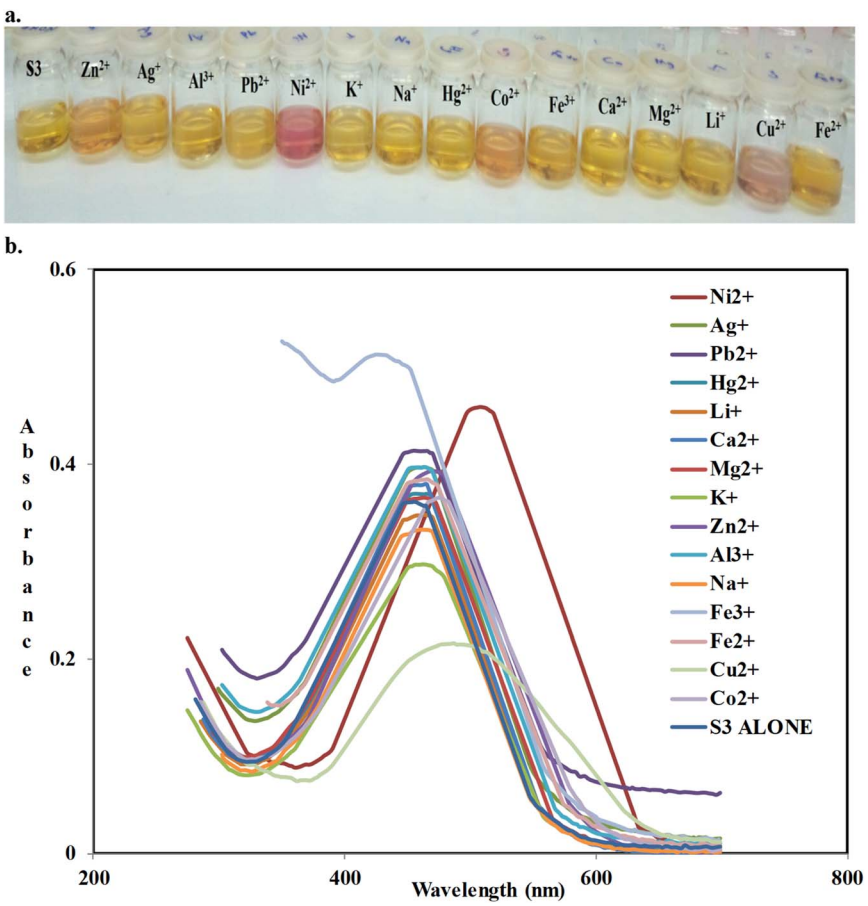

Fig. 6 Colour changes (a) and overlaid absorption spectra of nickel and other cations (b) in the presence of compound **S3** in ethanol : water (80 : 20, v/v).

Hg^{2+}, Li^{+}, Mg^{2+}, Na^{+}, K^{+}, Ag^{+}, Co^{2+}, Fe^{3+}, Fe^{2+}, and Al^{3+}. In the presence of compounds **S1**, **S5** and **S7**, none of the metal ions, including nickel ions, showed a peak where the difference in absorptivity was maximal (Fig. S27, S30 and S32 ESI†). For further analysis of nickel using compounds **S2**, **S3**, **S4**, and **S6**, analytical wavelengths of 448, 513, 470, and 497 nm were selected, respectively, while further work could not be done with the other azo dyes.

3.3.1 Structure–property relationship of sensors. A good chemical sensor should be selective for an analyte over other similar analytes, and be able to determine the analyte concentration in real time.[27]

From the chemosensor screening using **S1–S7**, compounds **S1**, **S5**, and **S7** were not suitable as chemosensors for cation detection and quantitation. On the other hand, compounds **S2**, **S3**, **S4**, and **S6** could serve as chemosensors for nickel ions. Complex solutions of the dyes and nickel gave different colours and distinct spectral patterns compared with other interfering metal ions. Enhanced conjugation due to Ni^{2+} coordination to 8-hydroxyquinoline-based azo dyes might be responsible for the observed colour change and the emergence of an absorption peak at a long wavelength. In previous research, the Goswami group (2014)[20] reported that the sensor–nickel complex showed π-electron delocalization, thus reducing the energy gap between LUMO and HOMO. It is noteworthy that the presence of a nitro group on the benzenoid residue of the diazonium component, which was absent from compounds **S1**, **S5**, and **S7**, was a common characteristic of the chemical structures of compounds **S2**, **S3**, **S4**, and **S6**. The nitro group could have promoted conjugation in the chemical structures; therefore, this structural feature should be noted when designing sensors for colorimetric measurement of nickel.

3.3.2 Optimization studies

Diluting the solvent for the sensor–nickel(II) reaction. Absorption spectra of the nickel complex of compounds **S2–S4**, and **S6** in acetone, DMSO, ethanol, methanol, and water are shown in Fig. S33–S37 (ESI).† High absorption intensity was shown by all chemosensors in acetone and low absorptivity in water. This might be due to the stronger interaction of the complex with acetone than in water. Although acetone gave the highest absorptivity, ethanol was used for the chemosensing

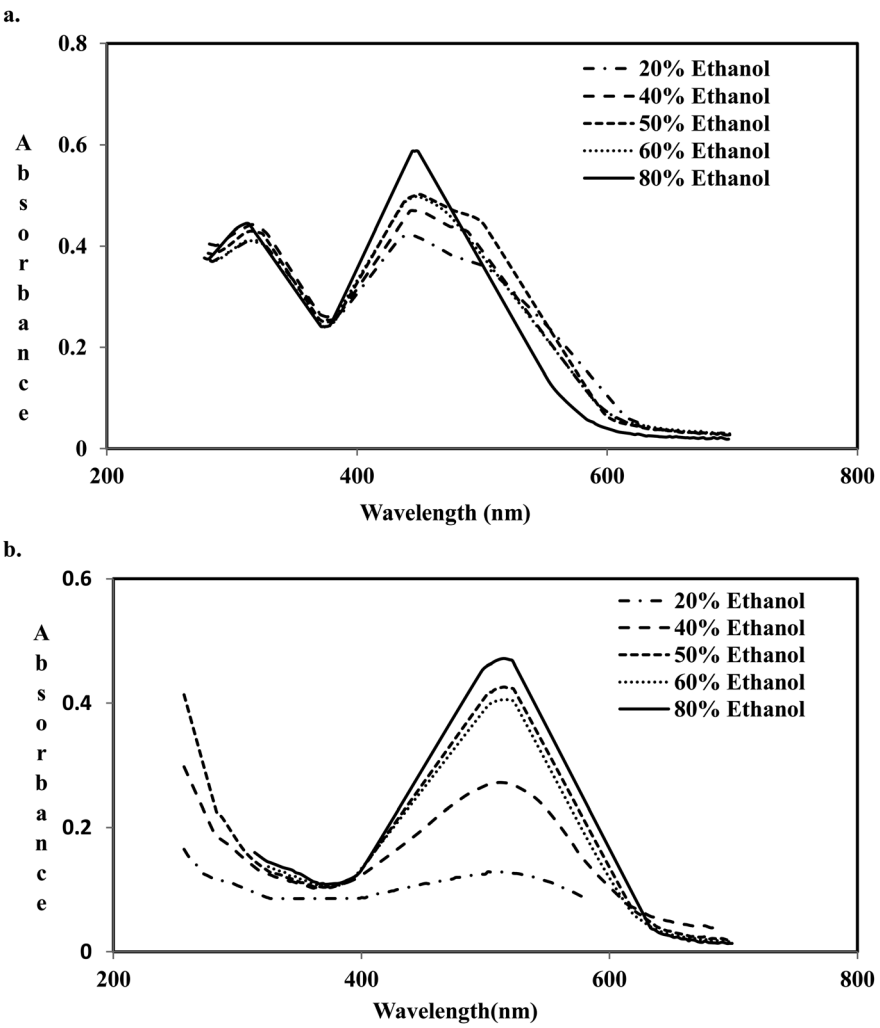

Fig. 7 Absorption spectra of compounds (a) S2, (b) S3 in the presence of nickel in different proportions of ethanol : water (80 : 20, v/v).

experiment in this study. Ethanol is cost-effective, readily available, and environmentally friendly.[28–32]

Sharma and co-workers (2016)[27] reported limited ionization of metallic salts in organic solvents. This might be the reason for the use of organic solvent–water binary mixtures as sensing milieus by the majority of methods.[16,17,33–36] Similarly, a binary chemosensing medium of organic solvent and water, comprising ethanol and water, was utilized in this work to solvate the cations. Ethanol/water (20%, 40%, 50%, 60%, and 80%) was added to replace the solvents, and UV-visible scans were recorded to select the best ethanol/water mixture.

As shown in Fig. 7, the absorption decreased as the water content rose. The increased polarity limited the solubility of the dye–nickel complex; and consequently, weak interaction with water. It was observed that complexes aggregated and precipitated on standing. Therefore, for chemosensing measurement, the proportion of 80% ethanol and 20% water that gave the highest absorbance intensity was selected.

Chelating time. The difference in the reaction time intervals on chelation between nickel and azo dyes was carried out at an incubation room temperature of 30 °C. Generally, as shown in Fig. 8, it was observed that the absorbance reached the maximum value at 2 minutes and declined steadily afterwards. This indicated that the chelating reaction was fast and completed after swirling the sensor/Ni^{2+} mixture for 10 seconds. Two minutes was used as the optimal chelating time.

3.3.3 pH effect. Azo compounds are sensitive to pH changes. In the presence of nickel, absorbance readings of compounds **S3**, **S4**, and **S6** were nearly the same in acidic conditions, unlike in basic conditions where there was a decline. Therefore, buffer pH 4 was selected for the determination of nickel using compounds **S3**, **S4**, and **S6** (Fig. 9). On the other hand, with compound **S2**, absorbance values are stable at basic pH. Therefore, the determination was done at pH 8.

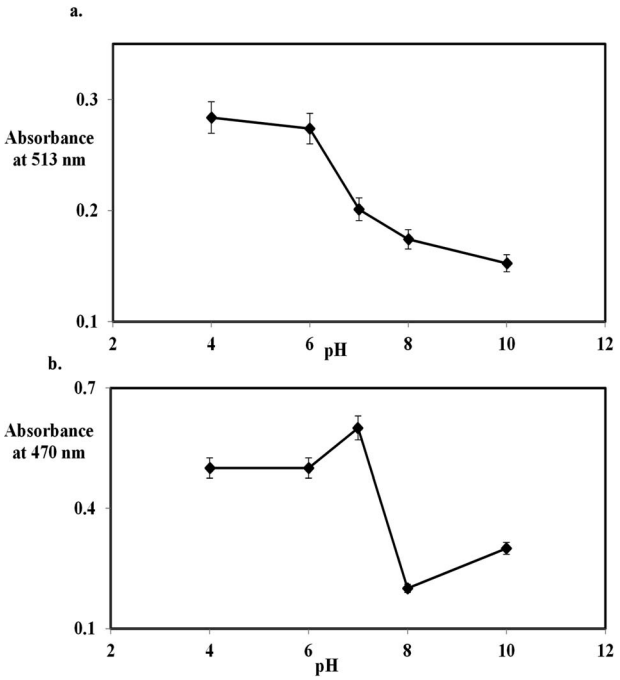

Fig. 9 Absorbance of compounds (a) **S3** (0.0154 mM) and (b) **S4** (0.0154 mM) in the presence of nickel ion at different pH values in ethanol : water (80 : 20, v/v).

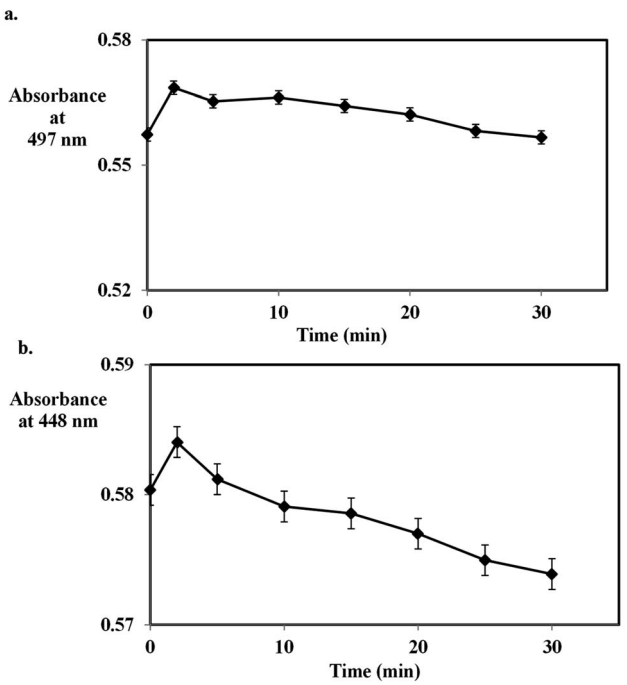

Fig. 8 Absorbance of compounds (a) **S6** (0.0161 mM) and (b) **S2** (0.0136 mM) in the presence of nickel ion at different time intervals in ethanol : water (80 : 20, v/v).

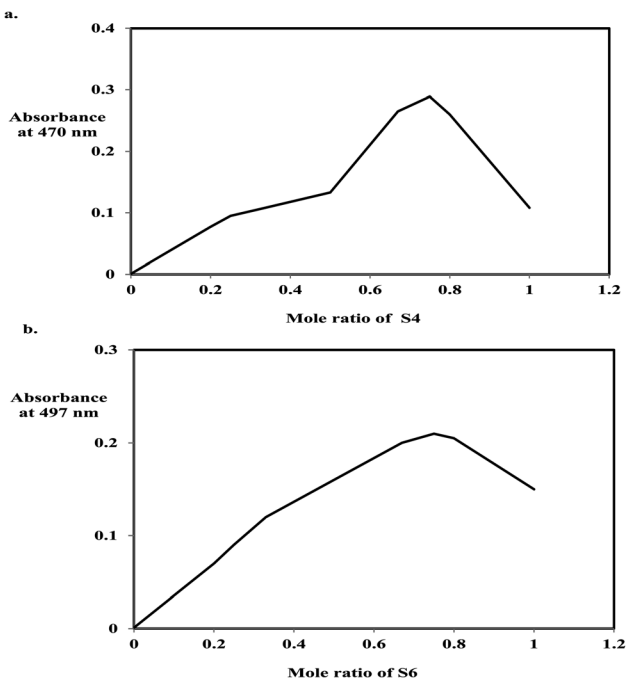

Fig. 10 Plot of the absorbance readings against the mole ratio of (a) **S4** and (b) **S6** in ethanol : water (80 : 20, v/v).

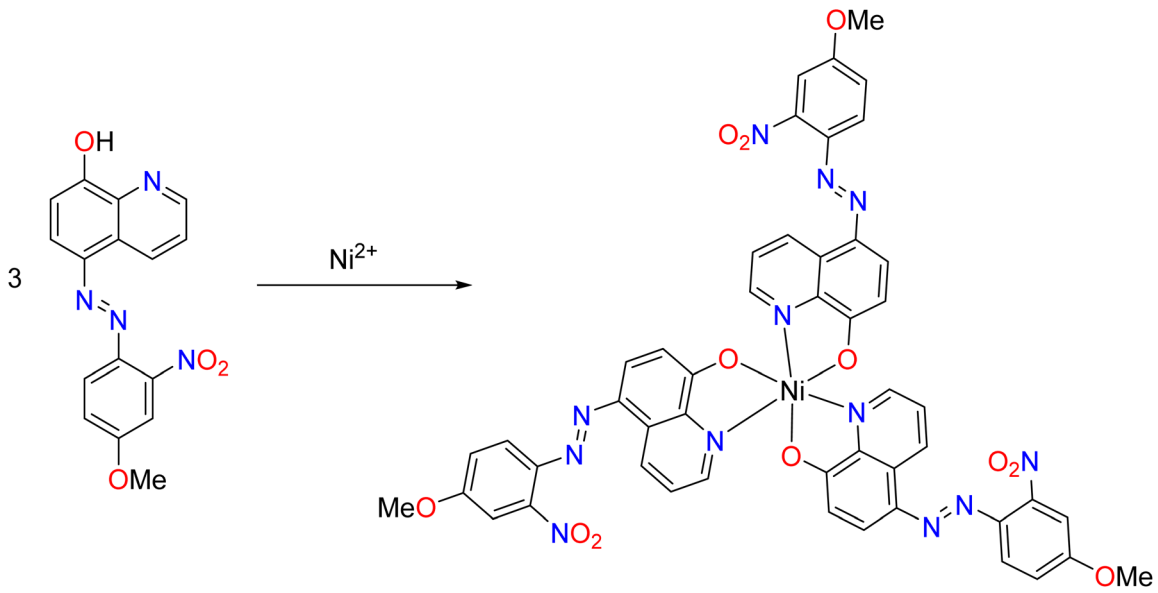

Fig. 11 Proposed reaction of the sensor with nickel ions.

3.3.4 Stoichiometry. The plot of the absorbance against the mole ratio of the sensor/Ni, as determined by Job's plot of continuous variation, was used to establish the sensor/Ni binding ratio. The plots for all the sensors reached a maximum value at a mole ratio of 0.75 (Fig. 10 and S40 ESI†). This indicated a 3 : 1 ratio of the sensor to Ni^{2+}.

With 3 mol of the ligands, oxygen and nitrogen in each mol of the sensors, electron pairs could be donated into the empty orbitals of nickel ions. Nickel has six coordination numbers in this case, and it is expected to be octahedral in shape. Fig. 11 shows the proposed product of sensor **S4** with nickel.

3.3.5 Validation parameters. The calibration plots showing the linearity of response of the absorbance with incremental addition of nickel ions are shown in Fig. S41 and S42 in the ESI.† The limits of detection (LODs) of the sensors ranged from 0.0116 to 0.0376 μM, as shown in Table 3; these indicated that the sensors would be useful for the determination of nickel ions at the nanomolar level. More so, these limits were lower than the majority of previously reported methods: Zhang group (2015),[15] Gupta and co-workers (2016),[37] Kumar group (2018),[19] and Manna *et al.* (2018)[33] reported 0.078, 0.696, 0.361, and 2.220 μM as limits of detection, respectively. This was an indication that the newly reported 8-hydroxyquinoline-based azo analysis had higher sensitivity than the majority of prior methods. However, the fluorescein-functionalized Fe_3O_4 nanoparticles reported by Shah and co-workers (2018)[13] showed a higher sensitivity, with an LOD of 0.83 nM. Equally, the Lei group (2014)[38] and Lv and his co-worker (2012)[39] developed nanomolar chemosensors for nickel detection at 2.4 and 5.0 nM limits, respectively.

Furthermore, the LODs of the new sensors were far less than the limit of 1.2 μM set for nickel ion detection by the United

Table 3 Analytical and validation parameters for the determination of nickel ions using the sensors

	Sensors			
Parameter	**S2**	**S3**	**S4**	**S6**
Analytical wavelength (λ_{max}, nm)	448	513	470	497
Range (μM)	1.35–5.40	1.54–4.63	1.54–6.17	1.61–6.45
Limit of detection (μM)	0.014	0.0376	0.0117	0.0116
Limit of quantitation (μM)	0.0459	0.1252	0.0389	0.0388
Sandell's sensitivity (nM per 0.001 absorbance unit)	45.30	6.18	12.41	12.26
Regression equation[a]				
Slope[b], *m*	0.0089	0.0652	0.0325	0.0329
95% confidence interval of slope	0.0012	0.0068	0.0080	0.0070
Intercept[b], *c*	0.3484	0.2332	0.1326	0.1011
95% confidence interval of slope	0.0206	0.0087	0.0100	0.0012
Correlation coefficient	0.9904	0.9959	0.9971	0.9953

[a] $y = mx + c$, where y is the absorbance for concentration × μM. [b] Three replicate determinations.

States Environmental Protection Agency.[40] This showed the high sensitivity of the sensor method.

3.3.6 Binding constant. Calculation of the binding constant (k) between nickel ions and sensors (**S2**, **S3**, **S4**, and **S6**) from plots of $\frac{1}{A-A_o}$ against $\frac{1}{[Ni^{2+}]}$ gave 4.181×10^4, 2.816×10^3, 1.151×10^4 and 1.09×10^3 M^{-1}, respectively. The k values follow the trend **S6** < **S3** < **S4** < **S2**. The highest value of K for compound **S2** is connected to the electron delocalization by the two nitro groups on the sensor. The binding constants were in the order of 10^3 to 10^4 M^{-1}. These values are in agreement with previously reported methods.

3.3.7 Competition experiments. Competition experiments were carried out to study the effect of interfering cations on the determination of nickel using the sensors. One main drawback of nickel determination was its competition with other first-row paramagnetic transition metals, especially copper and cobalt, that bind tightly to ligands relative to nickel.

The closeness of the absorbance values using compound **S2** revealed that nickel could be determined in the presence of other cations. The visual inspection of colour changes alluding to this property is shown in Fig. S43 (ESI).† On the contrary, Cu^{2+} ions interfered significantly with the determination of Ni^{2+} using sensors **S6** and **S3**, while a slight interference occurred for compound **S4**. Also, the colour changes affirmed this finding, as illustrated in Fig. 12, S44 and S45.† A similar interference in nickel determination in the presence of copper has been reported previously in the literature.[15,33,41,42] A rhodamine-based chemosensor developed by Abebe and co-workers (2011)[43] could only determine nickel in the absence of cobalt.

3.3.8 Determination of accuracy and precision of Ni^{2+} with sensors. The level of Ni^{2+} present in the blank tap and underground water was zero, as determined by the sensor and instrumental methods. The inter-day and intra-day accuracies and precisions for spike analysis in the tap and underground water samples determined by recovery studies and relative standard deviation (RSD), respectively, are presented in Tables 4–6 and S1–S6 (ESI).† The recoveries are between 99.39% and 104.86%, while the RSD values ranged from 1.00 to 2.94 for all of the azo dyes. A RSD value of less than 5% indicated the high precision of the methods (Tables 4–6).

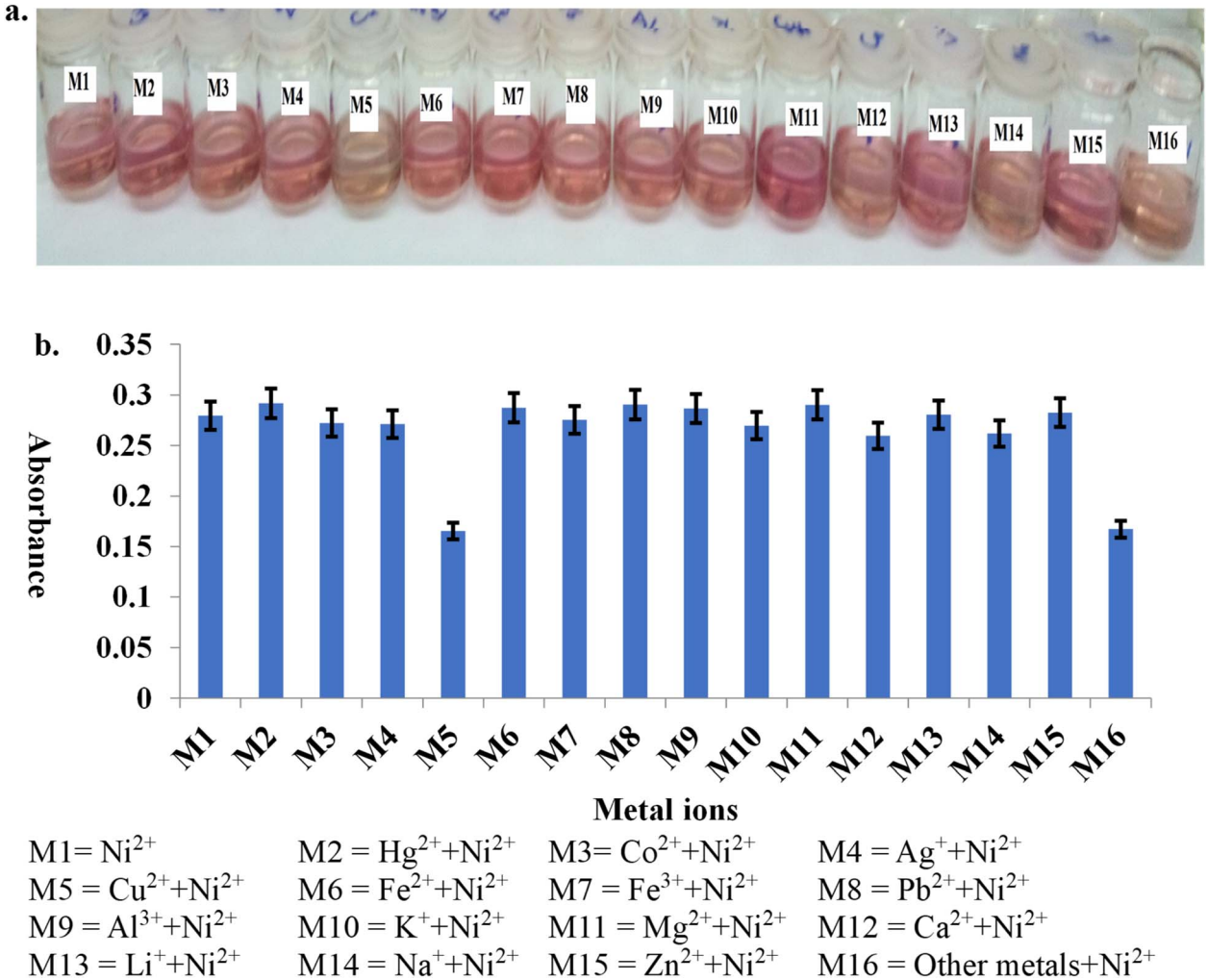

Fig. 12 Colours of sensor **S3** in the presence of Ni^{2+} and other metal ions (a), and the absorbance reading of mixtures at 513 nm (b).

Table 4 Inter-day accuracy and precision for the determination of Ni^{2+} using sensor **S2**

Water source	Amount added (μM)	% recovery[a] ± SD	RSD
Tap	3.215	102.04 ± 0.074	2.244
	5.626	102.59 ± 0.058	1.001
Underground	3.215	101.90 ± 0.053	1.619
	5.626	101.75 ± 0.159	2.793

[a] Average of twelve determinations.

Table 5 Inter-day accuracy and precision for the determination of Ni^{2+} using sensor **S3**

Water source	Amount added (μM)	% recovery[a] ± SD	RSD
Tap	1.607	101.66 ± 0.017	1.055
	3.215	103.26 ± 0.035	1.052
Underground	1.607	102.26 ± 0.024	1.464
	3.215	101.42 ± 0.096	2.938

[a] Average of twelve determinations.

Table 6 Percentage recovery of Ni^{2+} in tap and underground water determined by ICP-MS

Water source	% recovery ± SD[a]	RSD
Tap	100.78 ± 1.70	1.69
Underground	98.73 ± 1.75	1.77

[a] Average of six determinations.

3.3.9 Test of equivalence of the chemosensor probes and ICP-MS. The *F*-test was used to estimate the difference in variance between the sensor method and ICP-MS, while the *t*-test was used to compare the means. A 95% confidence limit was used in both cases, denoting a probability of 5%, *i.e.*, $p < 0.05$ of the null hypotheses. The *F*-test compared precision, while the *t*-test compared accuracy.

Table 7 shows the *t*-test and *F*-test values for sensors (**S2**, **S3**, **S4**, and **S6**), respectively. The *t*-test for the tap water sample ranged from 0.093 to 0.277, while the underground sample ranged from 0.051 to 0.088. The results of the *t*-test from both samples showed that there was no significant difference in accuracy, with *P* greater than 0.05. Therefore, the sensor and ICP-MS methods were equivalent in terms of the mean.

The *F*-test values for tap and underground water samples were 0.139–0.657 and 0.158–0.941 respectively. In both samples, these values were greater than 0.05. This indicated that there was no significant difference in the precision of the methods. Hence, they were equivalent in terms of variance.

3.3.10 Binding mechanism between Ni^{2+} and the sensor. In order to understand the mode of interaction of Ni^{2+} and the sensors, the FTIR spectra of the nickel complex of sensors and the sensors were superimposed to check for subtle differences in the vibrational frequencies. Using sensor **S2** as an example, the broad OH peak at around 3268 cm^{-1} in chemosensor **S2** disappeared in the nickel complex. The quinoline C=N peak in **S2** + Ni^{2+} appeared at 1594 cm^{-1}, while in **S2**, the peak was at 1610 cm^{-1}. The C–O vibrational frequencies at 1384 cm^{-1} and 1402 cm^{-1} appeared for **S2** and complex, respectively (Fig. 13). Other sensors interacted with nickel ions in a similar version. It could be deduced that the sensors interacted with Ni^{2+} through metal-to-ligand charge transfer *via* the hydroxyl and nitrogen groups of the hydroxyquinoline.

3.3.11 Paper strip tests. With compound **S3** as an example, the orange filter paper of **S3** changed to pink when dipped in nickel solution (Fig. 14). The ability of the sensors to change colour in a solid state similar to the liquid-phase reaction was an indication that they could be applied in the form of test strips for the real-time detection of nickel.

3.3.12 Comparison of the new sensor method with prior approaches. (1) The low concentration ranges reported in the 8-hydroxyquinoline azo dye analysis conferred higher sensitivity to the method than other methods.[18,19,33,44,45]

Table 7 Test of the equivalence of the sensor and ICP-MS method

Water source	*T*-test	*F*-test
S2 method		
Tap	0.277	0.657
Underground	0.071	0.543
S3 method		
Tap	0.246	0.139
Underground	0.088	0.941
S4 method		
Tap	0.116	0.178
Underground	0.051	0.158
S6 method		
Tap	0.093	0.568
Underground	0.060	0.855

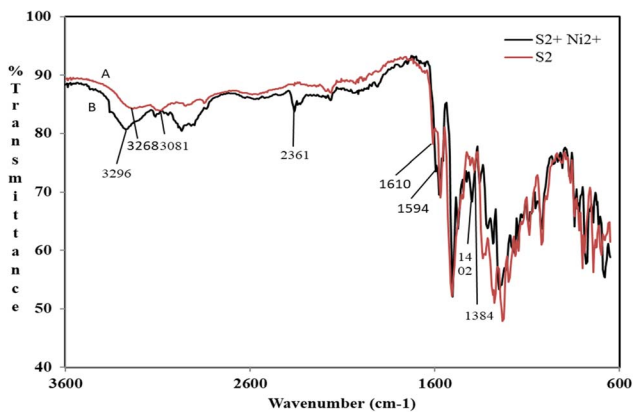

Fig. 13 Superimposed FTIR spectra of (A) sensor **S2** on (B) sensor **S2** + Ni^{2+}.

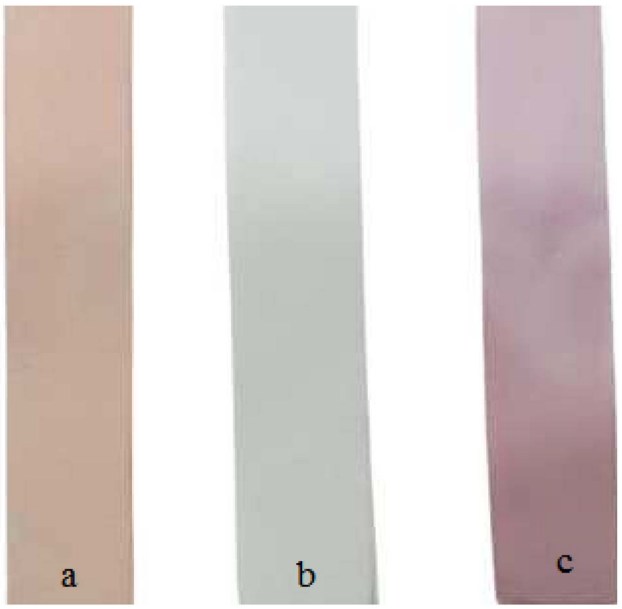

Fig. 14 Colours of the 1 cm × 5 cm filter paper (a) immersed in **S3** solution, (b) immersed in Ni^{2+} solution, and (c) air-dried paper coated with **S3** in Ni^{2+} solution in (b).

(2) The Li group (2012)[46] and Wang and co-workers (2012)[47] utilized coumarin as a structural motif to sense nickel, while the Ghosh group (2006)[48] and Maisonneuve and co-workers (2008)[49] reported the use of dipyrrin and benzothiazole, respectively. These structural motifs were synthesized through multiple steps and lengthy procedures. However, the azo dyes employed in this research were synthesized by two-step reactions: diazotization and diazocoupling.

(3) The 8-hydroxyquinoline-based azo dyes are simple and rapid sensors, with 0–2 min for the determination of nickel ions. Analytical time was gained compared to the methods of Lv and Luo (2012)[39] and Shrivas group (2017),[4] who reported incubation times of 30 and 5 min for the chelation of sensors and nickel ions, respectively.

(4) The use of a binary mixture of water and organic solvent as a chemosensing medium was common to the 8-hydroxyquinoline-based azo dyes and all the other chemosensor techniques. However, the Annaraj group (2016)[50] and Li and co-workers (2009)[42] reported the use of water as a medium for the chemosensing determination of nickel. Li *et al.*'s method used a glutathione-stabilized silver nanoparticle, and Annaraj *et al.*'s sensor has carboxyl as a water-solubilizing group. In some other methods, monosolvents were used; Chowdhury and co-workers (2018),[51] Xiang *et al.* (2014),[21] and the Gupta group (2016)[37] utilized acetonitrile, tetrahydrofuran, and dimethylsulfoxide, respectively. These solvents are not environmentally friendly, and they are more expensive relative to the ethanol used in this study.

4. Conclusion

Eight 8-hydroxyquinoline azo sensors were synthesized and characterized, of which compounds **S2**, **S3**, **S4**, and **S6** were suitable chemosensors for nickel. The optimized conditions were ethanol/water (80 : 20, v/v); pH 4 for compounds **S3**, **S4**, and **S6**, and pH 8 for compound **S2**; a reaction time of 2 minutes; and a stoichiometric ratio of 3 : 1. Infrared spectral analysis confirmed that sensors interacted with Ni^{2+} through quinoline nitrogen and hydroxyl moieties. Copper(II) ion interfered with Ni^{2+} determination using the sensors, except with compound **S2**. The sensor-based methods were of equivalent accuracy and precision to the ICP-MS method. The presence of a nitro group on the benzenoid residue of the diazonium component conferred selectivity on the sensors for nickel ion detection. The crystalline structure of the nickel complex of the azo dyes could not be obtained for X-ray crystallography. Furthermore, the detection and determination of nickel using the sensors could be limited by the high water content, as the complexes formed tend to aggregate and separate out on standing. Despite this, a simple, highly sensitive, and low-cost method of nickel analysis in water samples was established. The use of azo-based 8-hydroxyquinoline herein is the first described method for nickel ion detection and quantitation.

Data availability

The data used to support the findings of the study are available in the article.

Conflicts of interest

There are no conflicts to declare.

Acknowledgements

The authors are grateful to the Third World Academy of Sciences (TWAS) for the "Award of ICCBS-TWAS Sandwich Postgraduate Fellowship" (FR number: 3240316612) to S. O. O., and the Third World Center for Science and Technology (TWC), H. E. J. Research Institute of Chemistry, International Center for Chemical and Biological Sciences (ICCBS), Karachi, Pakistan.

References

1 B. Kaur, N. Kaur and S. Kumar, *Coord. Chem. Rev.*, 2018, **358**, 13–69.
2 B. Zambelli, F. Musiani, S. Benini and S. Ciurli, *Acc. Chem. Res.*, 2011, **44**, 520–553.
3 R. J. Maier, *Biochem. Soc. Trans.*, 2005, **33**, 83–85.
4 K. Shrivas, P. Maji and K. Dewangan, *Spectrochim. Acta, Part A*, 2017, **173**, 630–636.
5 S. C. Dodani, Q. He and C. J. Chang, *J. Am. Chem. Soc.*, 2009, **131**(50), 18020–18021.
6 S. C. Wilschefski and M. R. Baxter, *Clin. Biochem. Rev.*, 2019, **40**(3), 115–133.
7 D. Maity and T. Govindaraju, *Inorg. Chem.*, 2011, **50**, 11282–11284.
8 F. Sancenon, R. Martinez-Manez, M. A. Miranda, M. J. Segui and J. Soto, *Angew. Chem., Int. Ed.*, 2003, **42**(6), 647–650.

9 L. Zhao, D. Suib and Y. Wang, *RSC Adv.*, 2015, **5**(21), 16611–16617, DOI: 10.1039/C5RA00696A.
10 Y. Cheng, M. Zhang, H. Yang, F. Li, T. Yi and C. Huang, *Dyes Pigm.*, 2008, **76**(3), 775–783.
11 O. Arslan, B. Aydıner, E. Yalçın, B. Babür, N. Seferoğlu and Z. Seferoğlu, *J. Mol. Struct.*, 2017, **1149**, 499–509.
12 Y.-F. Cheng, Z.-Q. Liu, M. Shi, Q. Zhao, F.-Y. Li, T. Yi and C.-H. Huang, *Chin. J. Chem.*, 2007, **25**(5), 616–622.
13 M. T. Shah, A. Balouch and E. Alveroglu, *J. Mater. Chem.*, 2018, **6**, 1105–1115.
14 L. Lin, S. Hu, Y. Yan, D. Wang, L. Fan, Y. Hu and G. Yin, *Res. Chem. Intermed.*, 2017, **43**, 283–295.
15 I. Zhang, Y. Wang, C. Wan, Z. Xing, W. W. Li, M. Li and S. Zhang, *RSC Adv.*, 2015, **5**, 66416–66419.
16 A. Ashraf, M. Islam, M. Khalid, A. P. Davis, M. T. Ahsan, M. Yaqub, A. Syed, M. Abdallah, A. M. Elgorban, A. H. Bahkali and Z. Shafiq, *Sci. Rep.*, 2021, **11**(1), 1–13.
17 X. Liu, Q. Lin, T. Wei and Y. Zhang, *New J. Chem.*, 2014, **38**(4), 1418–1423.
18 G. Yang, X. Meng, S. Fang, L. Wang, Z. Wang, F. Wang, H. Duan and A. Hao, *New J. Chem.*, 2018, **42**, 14630–14641.
19 G. V. Kumar, M. P. Kesavan, M. Sankarganesh, K. Sakthipandi, J. Rajesh and G. Sivaraman, *New J. Chem.*, 2018, **42**, 2865–2873.
20 S. Goswami, S. Chakraborty, A. K. Das, A. Manna, A. Bhattacharyya, C. K. Quah and H. K. Fun, *RSC Adv.*, 2014, **4**, 20922–20926.
21 G. Xiang, L. Wang, W. Cui, X. An, L. Zhou, L. Li and D. Cao, *Sens. Actuators*, 2014, **196**, 495–503.
22 V. G. Voronin, I. D. Petrova, A. N. Leksin and B. V. Shemeryankin, *Pharm. Chem. J.*, 1976, **10**(9), 1215–1217.
23 J. S. Renny, L. L. Tomasevich, E. H. Tallmadge and D. B. Collum, *Angew. Chem., Int. Ed.*, 2013, **52**(46), 11998–12013.
24 O. E. Thomas and O. A. Adegoke, *J. Taibah Univ. Sci.*, 2022, **16**(1), 451–462.
25 J. Cai, Z. Li, Y. Qiu, Z. OuYang, W. Lin, L. Yang, W. Feng, X. Yu and W. Dong, *New J. Chem.*, 2016, **40**(11), 9370–9379.
26 H. Rashidnejad, M. Ramezanitaghartape, N. Pesyan, P. J. Mahon, M. M. Raposo, P. J. Coelho, A. Lup and A. Soltani, *J. Mol. Struct.*, 2021, **1223**, 129323.
27 H. Sharma, N. Kaur, A. Singh, A. Kuwar and N. Singh, *J. Mater. Chem. C*, 2016, **4**, 5154–5194.
28 D. R. Joshi and N. Adhikari, *J. Pharm. Res. Int.*, 2019, **28**(3), 1–18.
29 S. Kilo, T. Goen and H. Drexier, *Int. Arch. Occup. Environ. Health*, 2016, **89**(8), 1309–2320.
30 J. V. Ashurst and T. M. Nappe, *Methanol Toxicity*, Treasure Island (FL): StatPearls, 2023.
31 G. A. Burdock and I. G. Carabin, *Toxicol. Lett.*, 2004, **150**(1), 3–18.
32 Food and Drug Administration, *2018 Code of Federal Regulation, Title 21–Food and Drugs*, retrieved May 31, 2023, from, https://www.fda.gov.
33 A. K. Manna, J. Mondal, K. Rout and G. K. Patra, *Sens. Actuators*, 2018, **275**, 350–358.
34 G. Dhaka, N. Kaur and J. Singh, *Supramol. Chem.*, 2015, **27**(10), 654–660.
35 M. R. Ganjali, M. Hosseini, M. Motalebi, M. Sedaghat, F. Mizani, F. Faridbod and P. Norouzi, *Spectrochim. Acta, Part A*, 2015, **140**, 283–287.
36 M. Sahu, A. K. Manna, S. Chowdhury and G. K. Patra, *RSC Adv.*, 2020, **10**, 44860–44875.
37 V. K. Gupta, A. K. Singha, L. K. Kumawata and N. Mergu, *Sens. Actuators*, 2016, **222**, 468–482.
38 Y. Lei, H. Li, W. Gao, M. Liu, J. Chen, J. Ding, X. Huang and H. Wu, *J. Mater. Chem.*, 2014, **2**, 7402–7410.
39 X.-L. Lv and S.-Z. Luo, *Anal. Bioanal. Chem.*, 2012, **402**, 2999–3002.
40 M. Dhanushkodi, G. G. Kumar, B. K. Balachandar, S. Sarveswari, S. Gandhi and J. Rajesh, *Dyes Pigm.*, 2020, **173**, 1–29.
41 R. Joseph, B. Ramanujam, H. Pal and C. P. Rao, *Tetrahedron Lett.*, 2008, **49**, 6257–6261.
42 H. Y. Li, S. Gao and Z. Xi, *Inorg. Chem. Commun.*, 2009, **12**(4), 300–303.
43 F. Abebe, C. Eribal, G. Ramakrishna and E. Sinn, *Tetrahedron Lett.*, 2011, **52**, 5554–5558.
44 J. H. Kang, Y. S. Lee, H. M. Ahn and C. Kim, *Sens. Actuators*, 2017, **242**, 25–34.
45 S. Babaee, S. G. Pakdehi and A. S. Nabavi, *J. New Dev. Chem.*, 2016, **1**, 58–69.
46 H. Li, L. Cai and Z. Chen, *Adv. Chem. Sens.*, 2012, **1**, 121–150.
47 L. Wang, D. Ye and D. Cao, *Spectrochim. Acta, Part A*, 2012, **90**, 40–44.
48 S. K. Ghosh and T. Pal, *Chem. Rev.*, 2007, **107**(11), 4797–4862.
49 S. Maisonneuve, Q. Fang and J. Xie, *Tetrahedron*, 2008, **64**(37), 8716–8720.
50 B. Annaraj, L. Mitu and M. A. Neelakantan, *J. Mol. Struct.*, 2016, **1104**, 1–6.
51 B. Chowdhury, M. Karar, S. Paul, M. Joshi, A. Choudhury and B. Biswas, *Sens. Actuators*, 2018, **276**, 560–566.